



# Coordination Chemistry Reviews

journal homepage: [www.elsevier.com/locate/CCR](http://www.elsevier.com/locate/CCR)

## Review

# Design and construction of coordination polymers with mixed-ligand synthetic strategy

Miao Du <sup>a,\*</sup>, Cheng-Peng Li <sup>a</sup>, Chun-Sen Liu <sup>b</sup>, Shao-Ming Fang <sup>b,\*</sup><sup>a</sup> College of Chemistry, Tianjin Key Laboratory of Structure and Performance for Functional Molecule, Tianjin Normal University, Tianjin 300387, PR China<sup>b</sup> Zhengzhou University of Light Industry, Henan Provincial Key Laboratory of Surface & Interface Science, Zhengzhou, Henan 450002, PR China

## Contents

1. Introduction.....	1283
2. Assembly strategies of mixed-ligands in the construction of CPs .....	1284
2.1. Acid-acid mixed-ligand CPs.....	1284
2.2. Base-base mixed-ligand CPs.....	1285
2.3. Acid-base mixed-ligand CPs .....	1285
2.3.1. Spacer effect .....	1286
2.3.2. Positional isomeric effect.....	1291
2.3.3. Substituent effect.....	1294
3. Other factors influencing the assembly of mixed-ligand CPs .....	1296
3.1. Solvent.....	1297
3.2. pH condition .....	1298
3.3. Metal ion .....	1298
3.4. Synthetic route .....	1299
4. Construction of specific CPs with mixed ligands .....	1299
4.1. Unusual topological networks .....	1299
4.2. Entangled networks .....	1300
4.3. Chiral networks .....	1300
5. Physicochemical properties and applications .....	1301
5.1. Gas adsorption and separation.....	1301
5.2. Magnetism.....	1302
5.3. Catalysis .....	1302
6. Conclusion .....	1303
Acknowledgments .....	1304
References .....	1304

**Abbreviations:** CPs, coordination polymers; MOFs, metal-organic frameworks; SBU, secondary building unit; H<sub>2</sub>tp, terephthalic acid; H<sub>3</sub>tcb, 1,3,5-tris(4-carboxyphenyl)benzene; DEF, N,N'-diethylformamide; DMA, N,N'-dimethylacetamide; DMF, N,N'-dimethylformamide; 2,6-H<sub>2</sub>ndc, naphthalene-2,6-dicarboxylic acid; H<sub>2</sub>bpdc, 4,4'-biphenyldicarboxylic acid; R-H<sub>2</sub>man, R-mandelic acid; S-H<sub>2</sub>lac, S-lactic acid; Hamtaz, 3-amino-1H-1,2,4-triazole; H<sub>2</sub>aztz, 3,3'-azobis(1,2,4-triazole); H<sub>2</sub>ox, oxalic acid; H<sub>2</sub>sca, succinic acid; H<sub>2</sub>ada, adipic acid; H<sub>2</sub>sba, suberic acid; H<sub>2</sub>aza, azelaic acid; H<sub>2</sub>sea, sebacylic acid; bpy, 4,4'-bipyridine; bimb, 1,4-bis(imidazol-1-yl)-butane; 4,4'-bpt, 1H-3,5-bis(4-pyridine)-1,2,4-triazole; bpdb, 1,4-bis(4-pyridine)benzene; dfppb, 2,3-difluoro-1,4-bis(4-pyridine)benzene; bpeb, 1,4-bis(4-pyridineethynyl)benzene; bpee, 1,2-bis(4-pyridine)ethylene; bpea, 1,2-bis(4-pyridine)ethane; bpp, 1,3-bis(4-pyridine)propane; bib, 1,4-bis(imidazol-1-yl)-benzene; bix, 1,4-bis(imidazol-1-ylmethyl)benzene; bimx, 1,4-bis(imidazol-1-ylmethyl)-2,3,5,6-tetramethylbenzene; bie, 2,2'-bis(1H-imidazolyl)ether; bbi, 1,1'-(2,2'-oxybis(ethane-2,1-diy))bis(1H-imidazole); bte, bis(1,2,4-triazole-1-yl)ethane; btp, 1,3-bis(1,2,4-triazol-1-yl)propane; btb, 1,4-bis(1,2,4-triazol-1-yl)butane; tbmb, 1,4-bis(1,2,4-triazol-1-yl)methylbenzene; flu, 2-(2,4-difluorophenyl)-1,3-bis(1,2,4-triazol-1-yl)propan-2-ol; H<sub>2</sub>ip, isophthalic acid; bptz, 3,6-bis(4-pyridine)-1,2,4,5-tetrazine; bpae, 1,4-bis(4-pyridine)acetylene; bpbb, 1,1'-(4-butenediy)-bis(2-(2-pyridine)benzimidazole); hbpb, 1,1'-(6-hexanediy)-bis(2-(2-pyridine)benzimidazole); dbpb, 1,1'-(1,10-decanediy)-bis(2-(2-pyridine)benzimidazole); H<sub>2</sub>pa, phthalic acid; bpmpb, 2,2'-bis(4-pyridinemethyleneoxy)-1,1'-biphenylene; 2,3-H<sub>2</sub>ndc, naphthalene-2,3-dicarboxylic acid; azpy, 4,4'-azopyridine; H<sub>2</sub>oba, 4,4'-oxybis(benzoic) acid; pytz, 3,6-bis(pyridin-4-yl)-1,2,4,5-tetrazine; H<sub>3</sub>nbtc, 5-nitro-1,2,3-benzenetricarboxylic acid; H<sub>8</sub>tdpm, tetrakis[3,5-dicarboxyphenoxy]methylmethane; 4,4'-abpt, 4-amino-3,5-bis(4-pyridine)-1,2,4-triazole; o/m/p-H<sub>2</sub>pdpa, 1,2/1,3/1,4-phenylenediacetic acid; 4-bpo, 2,5-bis(4-pyridine)-1,3,4-oxadiazole; 3-bpo, 2,5-bis(3-pyridine)-1,3,4-oxadiazole; H<sub>3</sub>sp, 5-sulfosophthalic acid; 3,4'-bpt, 1H-3-(3-pyridine)-5-(4-pyridine)-1,2,4-triazole; 3,3'-bpt, 1H-3,5-bis(3-pyridine)-1,2,4-triazole; 3,3'-abpt, 4-amino-3,5-bis(3-pyridine)-1,2,4-triazole; H<sub>2</sub>nip, 5-nitroisophthalic acid; H<sub>3</sub>tma, trimesic acid; H<sub>2</sub>mip, 5-methylisophthalic acid; H<sub>2</sub>moip, 5-methoxyisophthalic acid; H<sub>2</sub>tbip, 5-(tert-butyl)isophthalic acid; H<sub>2</sub>hip, 5-hydroxyisophthalic acid; bpe, trans-1-(2-pyridine)-2-(4-pyridine)ethylene; H<sub>2</sub>atp, 2-aminoterephthalic acid; H<sub>2</sub>btp, 2-bromoterephthalic acid; H<sub>4</sub>bptc, 3,3',4,4'-benzophenonetetracarboxylic acid; H<sub>2</sub>tbtp, tetrabromoterephthalic acid; H<sub>2</sub>tfpbpp, N,N'-(2,3,5,6-tetrafluoro-1,4-phenylene)bis(methylene)bis(pyridine-4-carboxamide); H<sub>2</sub>fp, 5-fluoroisophthalic acid; H<sub>3</sub>btc, 1,2,4-benzenetricarboxylic acid; tib, 1,3,5-tris(1-imidazolyl)benzene; L-asp, L-aspartate; (+)-H<sub>2</sub>cam, (+)-camphoric acid; dabco, diazabicyclo[2.2.2]octane; H<sub>2</sub>cdc, 1,4-cyclohexanedicarboxylic; H<sub>2</sub>fma, fumaric acid; pyz, pyrazine; Hdhbc, 2,5-dihydroxybenzoic acid; H<sub>2</sub>pzdc, pyrazine-2,3-dicarboxylic acid; bpg, 1,2-bis(4-pyridine)glycol; H<sub>2</sub>mmal, 2-methylmalonic acid; H<sub>2</sub>mal, malonic acid; H<sub>2</sub>nndc, 1,5-dinitronaphthalene-3,7-dicarboxylic acid; H<sub>2</sub>suc, succinic acid; H<sub>2</sub>glu, glutaric acid; H<sub>2</sub>adi, adipic acid; H<sub>2</sub>pydc, pyridine-2,3-dicarboxylic acid.

\* Corresponding authors.

E-mail addresses: dumiao@public.tpt.tj.cn (M. Du), smfang@zzuli.edu.cn (S.-M. Fang).

## ARTICLE INFO

## Article history:

Received 15 June 2012

Accepted 1 October 2012

Available online 16 November 2012

## Keywords:

Coordination polymers

Crystal engineering

Mixed-ligand synthetic strategy

Structural diversity and regulation

Structure–property correlation

## ABSTRACT

The rational construction of coordination polymers (CPs), normally existing as infinite crystalline lattices extended from inorganic vertices and organic struts, essentially benefits from the development of crystal engineering strategies. In this review, we summarily comment on the key advances in the design of CPs using mixed-ligand synthetic strategy and discuss the relationship between the specifically selected mixed organic ligands and the resulting CPs. Significantly, fine tuning on the structural features of organic ligands, such as spacers, positional isomers, and substituents, can lead to a delicate regulation of the diverse network structures of CPs. Additionally, such mixed-ligand coordination assemblies may also be heavily affected by metal ion, synthetic route, and some other external stimuli such as solvent and pH condition, etc. The advantages of mixed-ligand systems as promising approaches to construct CPs-based crystalline materials with interesting structures and useful properties will also be demonstrated.

© 2012 Elsevier B.V. All rights reserved.

## 1. Introduction

The creation of new molecules is a major theme of chemistry, and of great contribution to human well-being and prosperity. Molecules are architectures of atoms, while crystal engineering of crystalline solids deals with targeted structures built from molecules [1,2]. As the prototype of polymeric crystal engineering, coordination polymers (CPs), in some cases also described as metal–organic frameworks (MOFs) [3], are an intriguing class of hybrid materials, which exist as infinite crystalline lattices extended from inorganic vertices (metal ions or clusters) and organic ligand struts by coordination interactions [4–6]. At this stage, the rational construction of structurally-defined CPs is quite successful and a variety of typical examples for such crystalline materials with attractive network architectures and potential applications have been reported. In this regard, their possible applications arising from the remarkable physicochemical properties of CPs are widely recognized in gas adsorption, molecular/ionic separation, optics, electricity, magnetism, chirality, catalysis, and drug delivery, etc. [7–12]. As a rule, the optimal implementation for such applications requires good phase purity, framework stability, and in some cases the available porosity of the targeted materials. Meanwhile, the crystalline nature of CPs materials allows for the unambiguous determination of crystal structures using X-ray diffraction technique and further, the proof-of-concept demonstration of structure–property correlation therein. In this context, a certain degree of structural design and prediction of CPs can be achieved through a detailed understanding of the building tectons involved, based on prior empirical observations, while their absolute structural control still remains a long-term goal and a worthwhile endeavor.

Much work has been devoted to the synthesis, structural characterization, and properties of CPs. In this process, the accumulation of sufficient experimental data allows chemists to proceed beyond the random studies and to derive some useful laws of assembly. Towards this end, several effective synthetic strategies such as ‘node-and-spacer’ [13,14] and ‘secondary building units (SBUs)’ [15,16] have been successfully established and developed, based on the notion that molecular precursors (metal ions and organic ligands) can be conveniently conceptualized as objects such as points, lines, polygons, and polyhedra, with CPs as periodic and complementary assemblies of these geometric motifs. Nevertheless, there are still many challenges in practice to perfectly project and regulate the specific crystal packing of such materials, because structural control will be readily thwarted by the intricate and non-covalent nature of the secondary interactions such as H-bonding, aromatic stacking, and van der Waals force, as well as some external physical or chemical factors including counterion, template, temperature, pressure, solvent, and pH value, etc. [17–25]. The vital theme in constructing CPs is to achieve a good junction between the organic tectons with adjustable connecting functions and the

inorganic metal ions with different coordination tendencies. Certainly, metal ions will play a central role in CPs, just as those in metallocopolymers [26–32]. However, in fact, they seem to be more regular in coordination assemblies, since the optional metal elements are limited to a specific range of the periodic table and will possess intrinsic coordination preferences with the given valences. As a consequence, major effort should be focused on the elaborate design and selection of a variety of organic ligands to realize the rational assembly and modulation of CPs.

To date, it is well known that multi-topic bridging ligands with two or more nitrogen, sulfur, phosphorus, and/or oxygen-involving functional groups can show different binding abilities to metal ions and thus can be applied as effective tectons for constructing diverse coordination networks [33]. However, in the scope of mixed-ligand CPs, ligands such as disulfoxide [34], dithioether [34], diphosphine [35], and hybrid *P,N*-type compounds [36] have seldom been used in practice, probably owing to the lack of competent counterparts as the co-ligands. In contrast, intense research activity towards the rational design and construction of mixed-ligand CPs has shown that the bipyridine and polycarboxyl compounds represent the most reliable and typical building blocks which can be jointly applied to synthesize a wide range of desired coordination networks. A choice of such connectors in coordination assembly can be rationalized based on the following considerations. On the one hand, the neutral bipyridine ligands normally bind to the metal ions as the rod-like bidentate tectons. On the other hand, polycarboxyl compounds may take the anionic or protonated form to provide various coordination modes upon binding to metals. Thus, the underlying structures of CPs obtained from a given bipyridine spacer can usually be ascribed to known geometrical networks, at least with hindsight, while assembly of a polycarboxyl bridging ligand with the metal ion under different conditions will lead to considerable structural complexity and diversity of CPs. As a result, by combining the advantages of two such types of ligands, the so-called mixed-ligand synthetic strategy can be rationally proposed. In this connection, Kitagawa and co-workers [37,38] have pioneered the synthesis of mixed-ligand CPs with pillared-layer microporous networks. Recently, this strategy has also been applied to design and prepare a series of carboxyl-functionalized porphyrin-based framework materials with diverse bipyridine pillarating linkers, which show emerging applications in gas storage, heterogeneous catalysis, and light harvesting [39].

According to the different compositions of mixed-ligand CP systems, they can be roughly classified into three categories: acid–acid, base–base, and acid–base systems (the concept of acid or base in this review only indicates the Lewis acid/base ligands). In the broad domain of CP study, coordination frameworks based on mixed ligands have been heavily developed. However, no specific structural prediction and design scheme is available at this stage. In this contribution, we will focus on current advances in CP systems with mixed bridging ligands, to demonstrate the significant

role of mixed-ligand synthetic strategies in defining the assemblies, structures, and properties of targeted CPs, and establish potential structure–property correlation for the rational design and construction of CPs in the future.

## 2. Assembly strategies of mixed-ligands in the construction of CPs

The strategic assembly of CPs involves both the macroscopic level and the microscopic scale. In this connection, the mixed-ligand assembly strategy facilitates the self-complement of reaction parameters at the macroscopic level, such as pH and solubility of the assembled system. While at the microscopic scale, the void positions around metal ions can be easily occupied by coordination with the mixed ligands, instead of solvents or anions; this may improve the stability of the resulting coordination architectures. Essentially, two different and compatible mechanisms may be applied to explain the formation of mixed-ligand CPs, when two ligand components are allowed to combine with the metal ions. On the one hand, each ligand will compete to interact with the metal center. On the other hand, they both serve as donors to coordinate with the same metal ion. As a result, the final CP products can be isolated and purified by crystallization. Actually, the mixed-ligand assembly strategy has been widely applied to design and synthesize numerous acid–base CPs. However, in the case of using two different ligands with similar coordination functionality (that is, acid–acid or base–base system), experimental data are so scarce that there is no basis to interpret even the most fundamental question (such as phase composition) for these systems.

### 2.1. Acid–acid mixed-ligand CPs

Previously, H<sub>2</sub>tp and H<sub>3</sub>tcb have been respectively used to react with Zn<sup>II</sup> to afford MOF-5 and MOF-177 under essentially identical synthetic conditions [40,41]. However, the assembly of both H<sub>2</sub>tp and H<sub>3</sub>tcb with Zn(NO<sub>3</sub>)<sub>2</sub> in DEF upon heating can give a new CP [Zn<sub>4</sub>O(tp)(tcb)<sub>4/3</sub>]<sub>n</sub> (**1a**) with hexagonal channels, which crystallizes in space group P6<sub>3</sub>m (see Fig. 1a) [42]. Interestingly, as the molar ratio of H<sub>3</sub>tcb is changed in the above mixed-ligand system, three different crystalline phases can be isolated. That is, at a low concentration of H<sub>3</sub>tcb, only MOF-5 is afforded; with increasing the ratio of H<sub>3</sub>tcb (H<sub>2</sub>tp:H<sub>3</sub>tcb = 4:1), needle crystals of **1a** are generated along with MOF-5. The optimal molar ratio of H<sub>2</sub>tp:H<sub>3</sub>tcb to form **1a** lies between 3:2 and 1:1. Along a further increment of H<sub>3</sub>tcb, MOF-5 decreases and MOF-177 appears, and when the molar ratio of H<sub>2</sub>tp:H<sub>3</sub>tcb reaches 2:3, MOF-177 first crystallizes from the reaction solution. These results clearly illuminate the competition and cooperation relationship between the H<sub>2</sub>tp and H<sub>3</sub>tcb components in coordination assemblies of CPs. By modifying the reaction routes (solvothermal reaction or room-temperature evaporation) and solvents (DMA or DMF), two additional CPs {[CH<sub>3</sub>)<sub>2</sub>NH<sub>2</sub>][Zn<sub>2</sub>(tp)(tcb)][Zn<sub>3</sub>(tcb)<sub>2</sub>(H<sub>2</sub>O)<sub>2</sub>](DMA)<sub>4</sub>(EtOH)<sub>2</sub>-(H<sub>2</sub>O)<sub>7</sub>]<sub>n</sub> (**1b**) and {[CH<sub>3</sub>)<sub>2</sub>NH<sub>2</sub>][Zn<sub>2</sub>(tp)(tcb)][(DMF)<sub>3</sub>(H<sub>2</sub>O)<sub>2</sub>]<sub>n</sub> (**1c**) can also be obtained [43]. In **1b**, two distinct polymeric networks with 2D 6<sup>3</sup> bilayers and 3D **hms** net (for the 3-letter network symbols, see ref. [44], the same below) are interpenetrated to result in an elaborate 2D + 3D framework (see Fig. 1b). While for **1c**, a 3-fold interpenetrating **gra** framework involving hexagonal chiral helical channels occurs (see Fig. 1c).

Of further interest, two homochiral porous CPs can be synthesized by heating Zn<sup>II</sup> nitrate, 2,6-H<sub>2</sub>ndc or H<sub>2</sub>bpdc with chiral R-H<sub>2</sub>man tecton [45]. By comparison, the assembly of Zn<sup>II</sup>, H<sub>2</sub>tp, and S-H<sub>2</sub>lac affords a 3D chiral CP, which shares the same topological isoreticular structure to the above two CPs, but with smaller pores [46]. Significantly, the different pore sizes and chiral centers

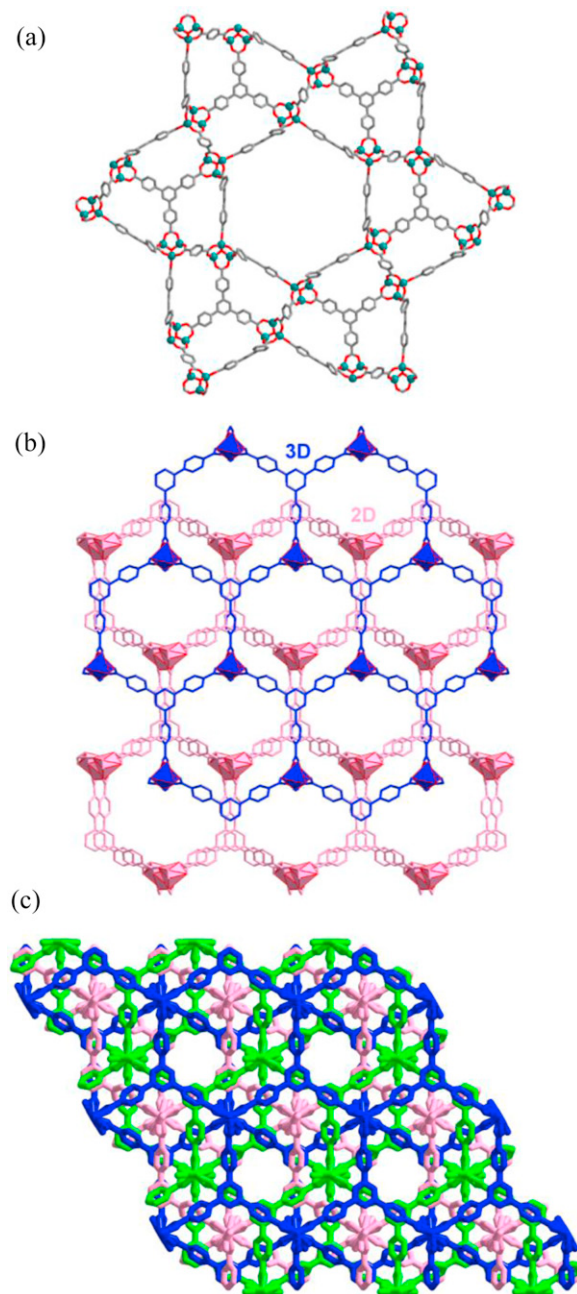


**Fig. 1.** (a) 3D network of [Zn<sub>4</sub>O(tp)(tcb)<sub>4/3</sub>]<sub>n</sub> (**1a**) showing 1D hexagonal channels [42]; (b) interpenetrating 2D+3D framework of {[CH<sub>3</sub>)<sub>2</sub>NH<sub>2</sub>][Zn<sub>2</sub>(tp)(tcb)][Zn<sub>3</sub>(tcb)<sub>2</sub>(H<sub>2</sub>O)<sub>2</sub>](DMA)<sub>4</sub>(EtOH)<sub>2</sub>(H<sub>2</sub>O)<sub>7</sub>]<sub>n</sub> (**1b**) [43]; (c) 3-fold interpenetrating framework of {[CH<sub>3</sub>)<sub>2</sub>NH<sub>2</sub>][Zn<sub>2</sub>(tp)(tcb)][(DMF)<sub>3</sub>(H<sub>2</sub>O)<sub>2</sub>]<sub>n</sub> (**1c**) [43].

result in distinct stereoselective sorption properties of the porous materials. That is, the larger pores will effectively and stereoselectively accommodate the bulkier guests, whereas the smaller pores show higher sorption and enantioselectivity toward the smaller chiral drug precursors. In addition, a highly selective oxidation of bulkier sulfides (2-NaphSMe (2-C<sub>10</sub>H<sub>7</sub>SMe) or PhSCH<sub>2</sub>Ph) will occur in the larger pores, which however is not allowed in the smaller ones.

Similar to those Lewis acids possessing the carboxyl groups, mixed H-triazole ligands can also be simultaneously combined in the same CP, which usually results from the *in situ* ligand synthesis reaction. For example, the hydrothermal treatment of Cd<sup>II</sup> with Hamtaz in H<sub>2</sub>O/NH<sub>3</sub>·H<sub>2</sub>O in the presence of Ag<sup>I</sup> at 130 °C,

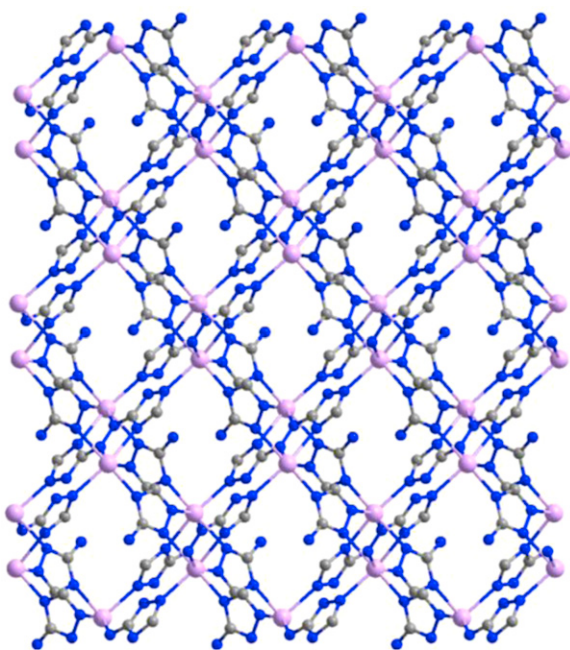
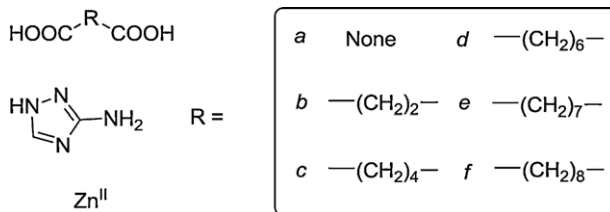


**Fig. 2.** 3D (3,4,5)-connected network of  $[Cd_2(\text{amtaz})_2(\text{aztaz})]_n$  (**2**) [47].

with the ratio of starting materials of 0.28:0.63:0.23, yields a homometallic CP  $[Cd_2(\text{amtaz})_2(\text{aztaz})]_n$  (**2**) [47]. This reaction can be regarded as Ag<sup>I</sup>-mediated *in situ* generation of aztaz<sup>2-</sup> from amtaz<sup>-</sup> through dehydrogenative coupling. In the resulting CP, the Cd<sup>II</sup> ions are linked by the mixed ligands to afford a complicated 3D (3,4,5)-connected network with  $(4.6^2)_2(4.6^7.8^2)_2(6^5.10)$  topology (see Fig. 2).

Combination of the *H*-triazole ligand Hamtaz and a series of comparable carboxylic acids with Zn<sup>II</sup> produces a family of 3D pillared-layer CPs [48]. This series of carboxylic acids include H<sub>2</sub>ox, H<sub>2</sub>sca, H<sub>2</sub>ada, H<sub>2</sub>sba, H<sub>2</sub>aza, and H<sub>2</sub>sea (Scheme 1, see a-f), which will show different bridging distances and corrugated



**Scheme 1.** Illustration of the mixed-ligand assembled system with Zn<sup>II</sup>, Hamtaz, and a series of comparable dicarboxylic acids, including (a) H<sub>2</sub>ox, (b) H<sub>2</sub>sca, (c) H<sub>2</sub>ada, (d) H<sub>2</sub>sba, (e) H<sub>2</sub>aza, and (f) H<sub>2</sub>sea.

conformations in pillaring the 2D  $[\text{Zn}(\text{amtaz})]_n$  layers into 3D networks (see Fig. 3). The structural characteristics of these CPs demonstrate that both the layers and pillars tend to flexibly constitute more compact lattice architectures, and their structural differentiation is mainly dependent on the lengths and geometries of the dicarboxylates.

## 2.2. Base-base mixed-ligand CPs

CPs with mixed neutral *N,N'*-bidentate ligands are quite rare and in this context, a typical example  $[\text{Co}(\text{bpy})(\text{bimb})(\text{SCN})_2]_n$  (**3**) is synthesized by hydrothermal reaction of mixed ligands bpy and bimb with Co(SCN)<sub>2</sub> [49]. In this structure, the 2D (4,4) layers of  $[\text{Co}_4(\text{bpy})_2(\text{bimb})_4]$  units are pillared by the bpy rods to produce a 3D framework, which has a trinodal 4-connected network of  $(6^4.8^2)(6^3.8^3)_2(6^5.8)$  topology. Two such nets are further entangled to afford a 2-fold interpenetrating pattern (see Fig. 4).

## 2.3. Acid-base mixed-ligand CPs

The acid-base system is the most important and flourishing branch of mixed-ligand CPs. Naturally, acid and base ligands are perfect partners that can compensate charge balance, coordination deficiency, repulsive vacuum, and weakly interaction all at once. In this context, it is valuable to propose the rational synthetic strategy to regulate the network structures of mixed-ligand CPs by ligand

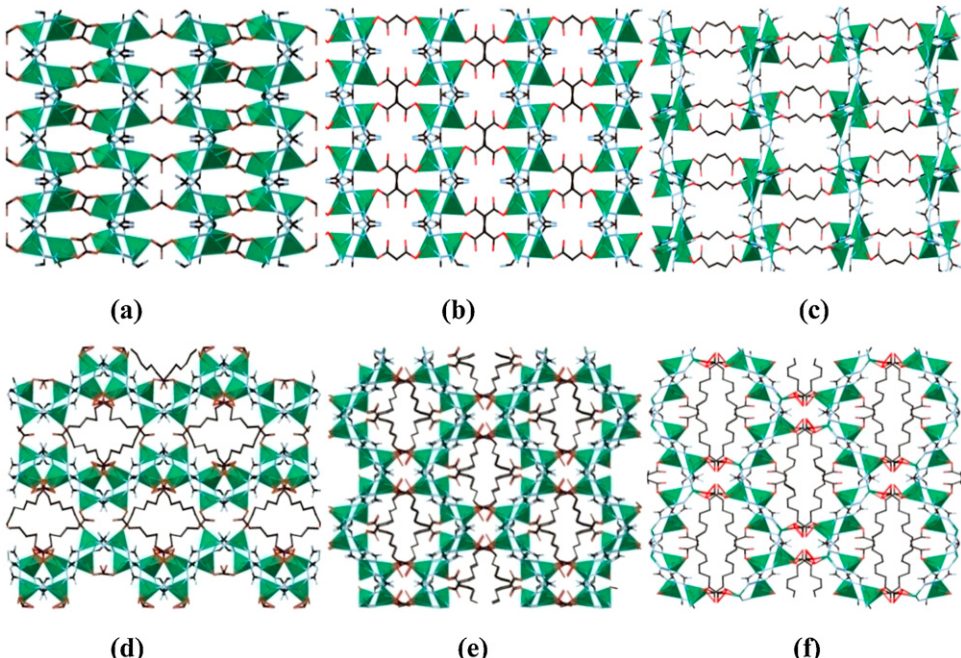


**Fig. 3.** Packing diagrams of the 3D pillared-layer networks constructing from Hamtaz and comparable carboxylic acids, including (a) H<sub>2</sub>ox, (b) H<sub>2</sub>sca, (c) H<sub>2</sub>ada, (d) H<sub>2</sub>sba, (e) H<sub>2</sub>aza, and (f) H<sub>2</sub>sea [48].

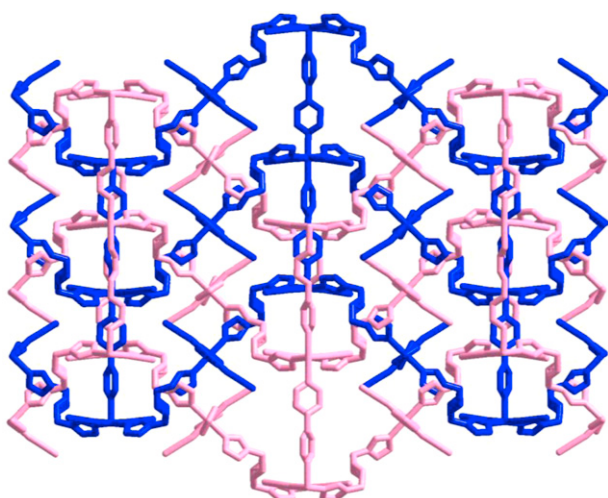
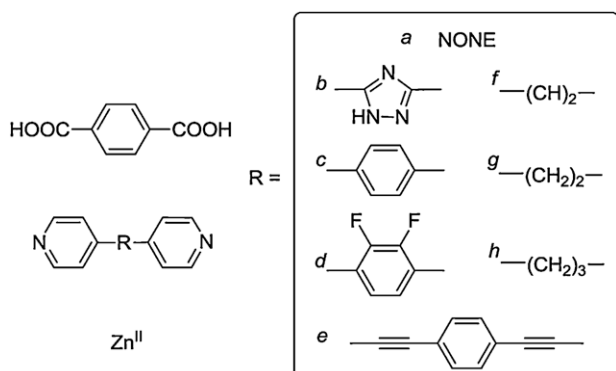


**Fig. 4.** Packing diagram of the 2-fold interpenetrating framework of  $[\text{Co}(\text{bpy})(\text{bimb})(\text{SCN})_2]_n$  (**3**) [49].

design or selection, considering the aspects of spacer effect, positional isomeric effect, and substituent effect of the organic building blocks.

### 2.3.1. Spacer effect

Generally, by deliberately modulating the nature of spacers between the functional coordinating groups of the bridging ligands, the resulting CP networks can be systematically and regularly adjusted. This strategy may permit a better understanding of the relationship between the nature of pillars and the pore sizes of CPs. Moreover, chemical or physical characteristics such as hydrophilicity/hydrophobicity, hydrogen bonds, and open metal sites can be achieved by introducing different functional pillars. In principle, rigid linkers tend to construct 3D open networks with available cavities. With the increase of spacer length, entanglement of such nets generally occurs to decrease the empty volumes of the crystal lattices. In contrast, flexible spacers may promote the generation



**Scheme 2.** Illustration of the mixed-ligand assembled system with  $\text{Zn}^{\text{II}}$ ,  $\text{H}_2\text{tp}$ , and a series of comparable bipyridyl ligands with different spacers, including (a) bpy, (b) 4,4'-bpt, (c) bpb, (d) dfbpb, (e) bpeb, (f) bpee, (g) bpea, and (h) bpp.

of distorted frameworks, leading to dynamic microporous CPs that can shrink or expand upon external stimuli.

$\text{H}_2\text{tp}$  and bpy can be viewed as the most popular acid and base bridging ligands for preparing CPs, which possess the paired functional groups (carboxyl and pyridine) in the two sides of their backbones. In this regard, hydrothermal reaction of  $\text{H}_2\text{tp}$ , bpy, and  $\text{Zn}^{\text{II}}$  affords a 2-fold interpenetrating 3D CP  $[\text{Zn}(\text{tp})(\text{bpy})]_n$  (**4a**), which contains parallelogram-like  $[\text{Zn}(\text{tp})]_n$  sheets and bpy pillars (see Fig. 5a) [50]. By introducing the spacers ( $R$ ) between the pyridine groups of bpy, a series of comparable bpy derivatives with extended and varied lengths can be obtained and have been extensively applied in the synthesis of mixed-ligand CPs (Scheme 2, see a–h).

On the one hand, a family of conjugated aromatic spacers can be used to design the longer rigid bipyridine ligands, including 4,4'-bpt [51], bpb [52], dfbpb [52], and bpeb [53], assemblies of which with  $\text{H}_2\text{tp}$  and  $\text{Zn}^{\text{II}}$  will afford a series of comparable 3D CPs of 2-fold interpenetrating pccu topological networks (**4b–4e**, see Fig. 5b–e). In the resulting 3D frameworks, though the pillar lengths vary from 7.04 Å (for bpy, **4a**), to 10.74, 11.47, 11.49, and 15.43 Å, the 2-fold interpenetrating structures of such CPs make their lattices more

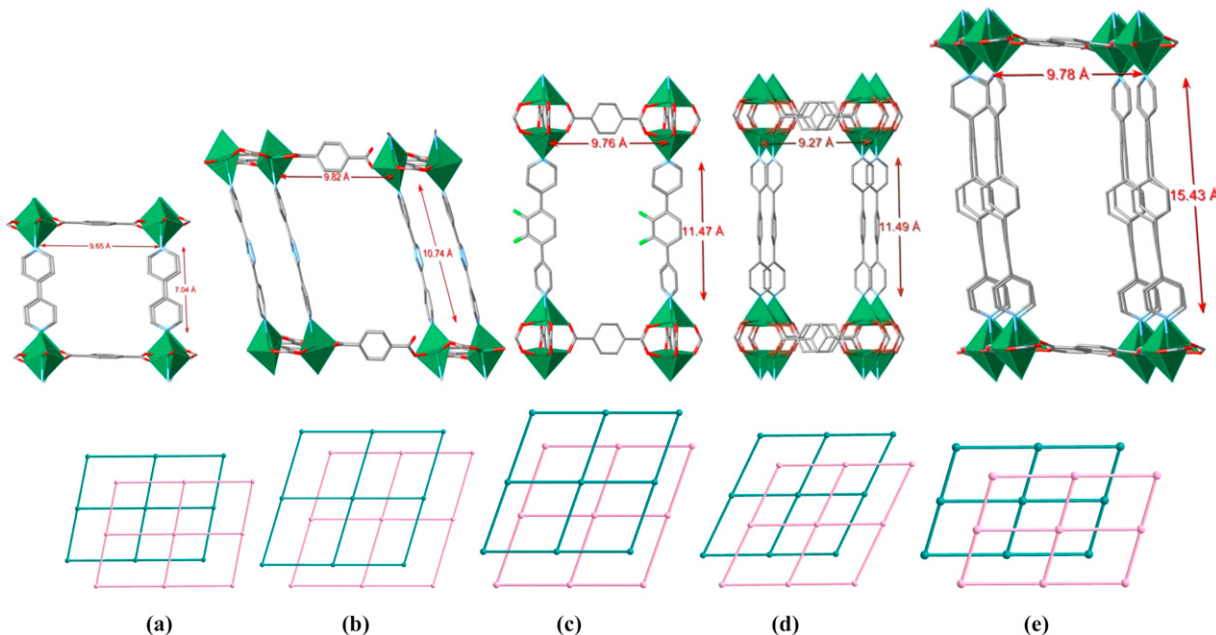


**Fig. 5.** Schematic illustration showing the different cubic frameworks pillared by (a) bpy [50], (b) 4,4'-bpt [51], (c) bpb [52], (d) dfbpb [52], and (e) bpeb [53] as well as their 2-fold interpenetrating arrangements (**4a–4e**).

compact, with the voids being 14.7% (for **4b**), 37.9% (for **4c**), 40.4% (for **4d**), and 26.5% (for **4e**) of the total lattice volumes. Generally, the longer the pillar is, the higher the void ratio is, as found in **4a–4d**. However, the void decreases significantly in **4e**, which can be attributed to a better packing efficiency of the independent nets.

On the other hand, regarding the changes of spacers with aliphatic groups, a series of flexible bipyridine ligands can be obtained, such as bppe, bpea, and bpp. Reactions of H<sub>2</sub>tp with

Zn<sup>II</sup> in the presence of these exo-extended ligands will result in more flexible coordination species. Notably, all Zn<sup>II</sup> ions in these CPs uniformly take the distorted tetrahedral coordination geometry. In the 3D polymeric pattern of **4f**, the Zn<sup>II</sup> centers are connected via bridging bppe and tp to form a 3D **dia** net with large cavity, which is further filled by interpenetration of four other independent and equivalent networks [54]. The assembly of bpea with H<sub>2</sub>tp and ZnCl<sub>2</sub> produces a 2D CP **4g** in which one

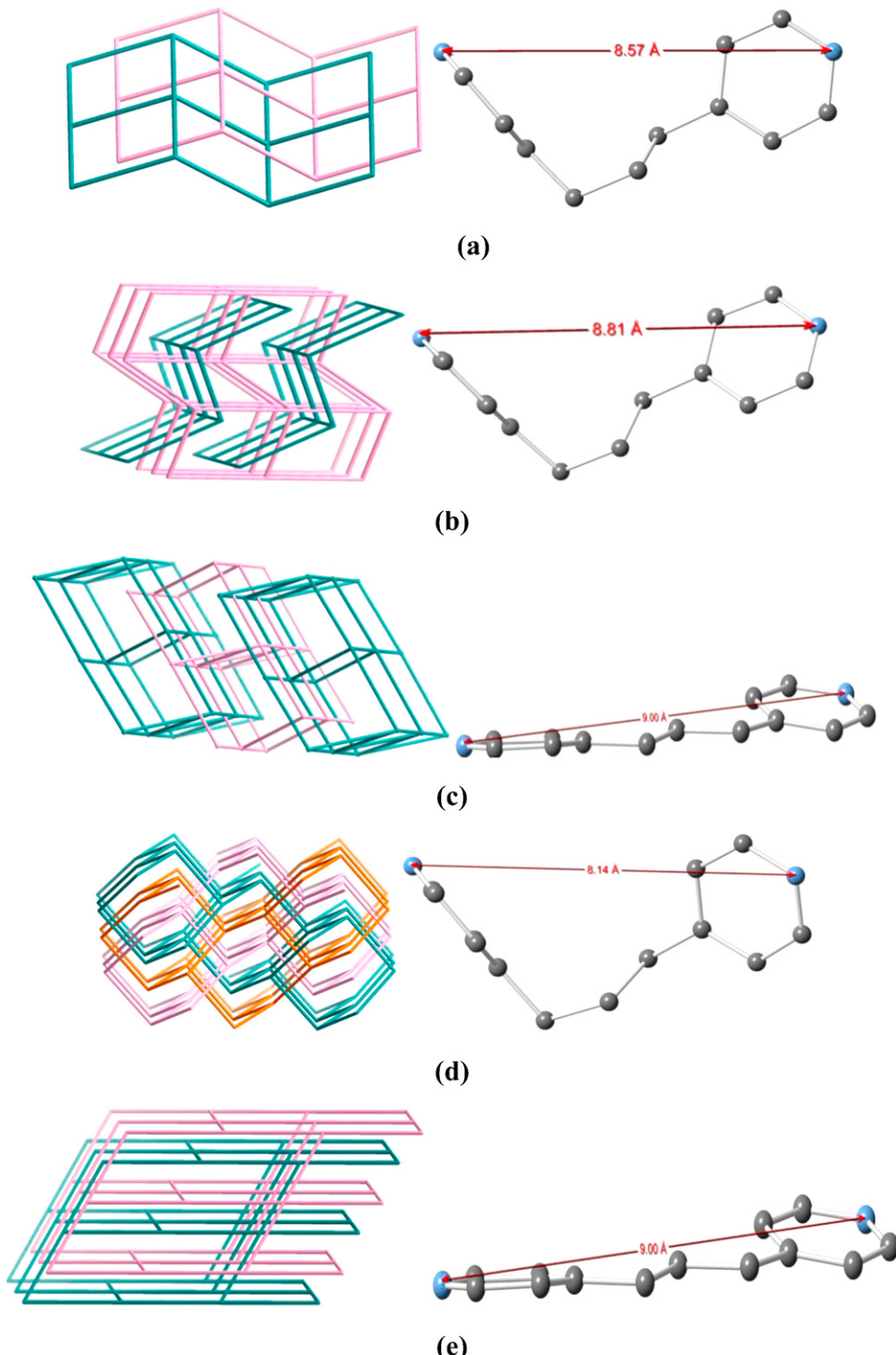
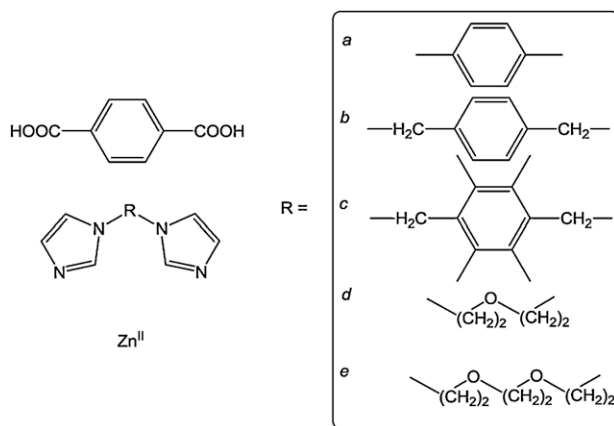


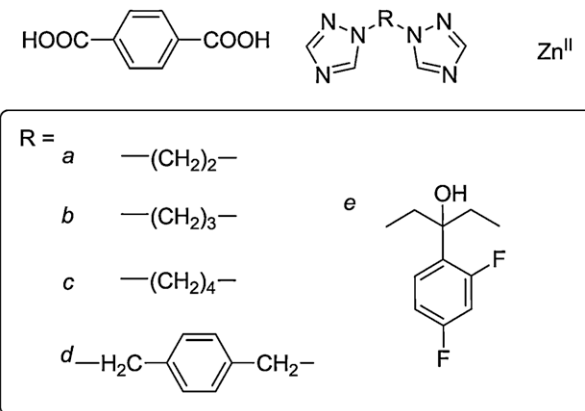
**Fig. 6.** Schematic illustration showing the distinct networks generated from Zn<sup>II</sup>, tp, and the flexible bpp ligand under different reaction conditions: (a) 2-fold interpenetrating 2D corrugated layers in **4h**<sup>1</sup> [56], (b) 2D + 2D inclined interpenetrating layers in **4h**<sup>2</sup> [57], (c) 2D parallel interpenetrating bilayer in **4h**<sup>3</sup> [57], (d) 3-fold interpenetrating **dia** framework in **4h**<sup>4</sup> [58], and (e) 2-fold interpenetrating **cds** topology in **4h**<sup>5</sup> [59].



chloride anion occupies a coordination site of  $Zn^{II}$  to prevent further structural extension [55]. Due to the greater flexibility of bpp, five distinct polymeric networks can be constructed under different conditions. For instance, the hydrothermal reaction of  $Zn^{II}$ ,  $H_2tp$ , and bpp under  $100^{\circ}C$  results in  $[Zn(tp)(bpp)]_n$  (**4h<sup>1</sup>**, see Fig. 6a), which shows the 2D corrugated layers of 2-fold interpenetration [56]. Interestingly, the assembly of  $Zn(NO_3)_2$ ,  $H_2tp$ , and bpp under a one-pot hydrothermal reaction at  $160^{\circ}C$  simultaneously yields two different products, namely, yellow diamond crystals of  $\{[Zn(tp)(bpp)]_2(H_2O)_2\}_n$  (**4h<sup>2</sup>**, see Fig. 6b) and white prism crystals of  $[Zn_4(tp)_4(bpp)_2]_n$  (**4h<sup>3</sup>**, see Fig. 6c), which exhibit the polycatenation feature of 2D + 2D inclined layers and parallel entanglement of 2D 6-connected bilayers, respectively [57]. By mixing two such ligands in alkaline conditions, a new CP  $\{[Zn(tp)(bpp)](H_2O)_2\}_n$  (**4h<sup>4</sup>**, see Fig. 6d) with a 3-fold interpenetrating 6<sup>6</sup> framework is afforded [58]. Unlike **4h<sup>2</sup>** and **4h<sup>3</sup>**, hydrothermal reaction of  $ZnCl_2$ ,  $H_2tp$ , and bpp at  $160^{\circ}C$  gives a 3D CP  $[Zn_2(tp)(bpp)Cl_2]_n$  (**4h<sup>5</sup>**, see Fig. 6e), which shows the 2-fold interpenetrating **cds** topological framework [59].

Taking bis-imidazolyl into consideration instead of bipyridine, the spacer effect on structural assemblies of CPs can also be observed (Scheme 3, see a–e). Hydrothermal reaction of  $Zn^{II}$ ,  $H_2tp$ , and bib affords a 3D **pcu** topological framework of 3-fold interpenetration (**5a**) [60]. By replacing the phenyl group with the more flexible *p*-bimethylphenyl spacer, two new CPs (**5b<sup>1</sup>** and **5b<sup>2</sup>**) constructed from  $Zn^{II}$ ,  $H_2tp$ , and bix are obtained under different reaction conditions, showing a 2D + 2D → 3D entangled pattern consisting of inclined layers and a 2D + 2D → 2D 3-fold parallel interpenetrating framework, respectively [61]. By further decorating the phenyl rings with four methyl substituents, two temperature-induced  $Zn^{II}$  CPs **5c<sup>1</sup>** and **5c<sup>2</sup>** involving tp and bimx can be synthesized under hydrothermal conditions [62]. **5c<sup>1</sup>** consists of stacking composited layers each being 2-fold interpenetrating 2D square grids, while **5c<sup>2</sup>** has a 3D **pcu** open framework with large channels that are occupied by  $H_2tp$  templates. Employing the more flexible bis-imidazolyl ligand with the  $-(CH_2)_2O(CH_2)_2-$  spacer (bie) in a similar assembled system yields a quite rare 3-fold interpenetrating **ths** framework (**5d**) [63]. Further enlarging the spacer to  $-(CH_2)_2O(CH_2)_2O(CH_2)_2-$  results in a significantly flexible bbi ligand, which can bridge the  $Zn^{II}$  centers with the aid of tp co-ligand to construct a uniform 8-connected (3<sup>6</sup>.4<sup>18</sup>.5<sup>3</sup>.6) net for **5e** with the trinuclear  $Zn^{II}$  clusters as SBUs [64].

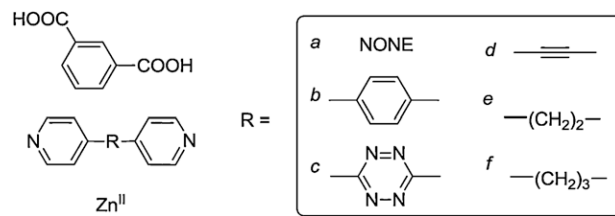
In the mixed-ligand CP systems with bis-triazolyl and  $H_2tp$ , the inserted spacers between two terminal triazolyl rings will clearly make the resulting ligands more flexible and adjustable (Scheme 4, see a–e). In  $\{[Zn(tp)(bte)](H_2O)_2\}_n$  (**6a**), the  $[Zn_2(bte)_2]$  binuclear



**Scheme 4.** Illustration of the mixed-ligand assembled system with  $Zn^{II}$ ,  $H_2tp$ , and a series of comparable bis-triazolyl ligands with different spacers, including (a) bte, (b) btp, (c) btb, (d) btmb, and (e) flu.

units are interlinked by the bridging tp ligands to generate a 2D rhombic network [65]. Diffusion reactions of  $Zn^{II}$  chloride or nitrate with mixed btp and  $H_2tp$  ligands lead to the formation of two different CPs  $\{[Zn(tp)(btp)][Zn(tp)_{0.5}(btp)Cl](H_2O)\}_n$  (**6b<sup>1</sup>**) and  $\{[Zn(tp)(btp)][CH_3OH](H_2O)_2\}_n$  (**6b<sup>2</sup>**) [66]. CP **6b<sup>1</sup>** features an interesting entangled pattern, in which half of the channels within the parallel 2D layers are polythreaded by 1D arrays, whereas **6b<sup>2</sup>** shows a familiar 2D 6<sup>3</sup> network. By changing the pH of the reaction medium, the assembly of  $Zn^{II}$ ,  $H_2tp$ , and btb can afford two distinct CPs  $\{[Zn_2(tp)_2(btbt)_2](H_2O)_2\}_n$  (**6c<sup>1</sup>**) and  $[Zn(tp)(btbt)_{0.5}]_n$  (**6c<sup>2</sup>**) based on tetrahedral and octahedral SBUs, respectively [67]. As a result, they show the 3-fold interpenetrating **dia** array and 3-fold interpenetrating **pcu** framework, respectively. When more bulky spacers are further introduced into the tectons, 2D CPs  $[Zn(tp)(btmb)]_n$  (**6d**) [68] and  $[Zn(tp)(flu)]_n$  (**6e**) [69] with polymeric grids can be constructed, probably due to the steric effect of aromatic spacer groups.

Various base-type bridging ligands, involving paired pyridine (Scheme 5, see a–f), imidazole, and triazole groups with different spacers in between, have also been applied to react with angular rigid dicarboxylic acids to form well-defined CPs, which can be regulated by the spacer effect of ligands. For example,  $H_2ip$  has been extensively used to construct CPs and those of  $Zn^{II}$ ,  $H_2ip$ , and bpy exhibit evident structural diversity. CPs  $\{[Zn(ip)(bpy)(H_2O)](H_2O)_{1.5}\}_n$  (**7a<sup>1</sup>**, see Fig. 7a) and  $\{[Zn_2(ip)_2(bpy)(EtOH)(H_2O)_2](EtOH)(H_2O)_{0.5}\}_n$  (**7a<sup>2</sup>**, see Fig. 7b) can be prepared under similar condition except for different molar ratios of the reactants, which show 2D square and 2D interpenetrating **hcb** networks, respectively [70]. For the hydrothermal reaction product  $[Zn_4O(ip)_3(bpy)]_n$  (**7a<sup>3</sup>**, see Fig. 7c), the tetranuclear SBUs bearing  $Zn_4O$  cores are extended by ip and bpy to construct a 2D network [71]. Hydrothermal reaction of  $Zn^{II}$ ,  $H_2ip$ , and bpy in alkaline solution gives a novel CP  $\{[Zn(ip)(bpy)_2][Zn(ip)(bpy)](H_2O)_{0.25}\}_n$  (**7a<sup>4</sup>**, see Fig. 7d), within



**Scheme 5.** Illustration of the mixed-ligand assembled system with  $Zn^{II}$ ,  $H_2ip$ , and a series of comparable bipyridyl ligands with different spacers, including (a) bpy, (b) bpb, (c) bptz, (d) bpae, (e) bpea, and (f) bpp.

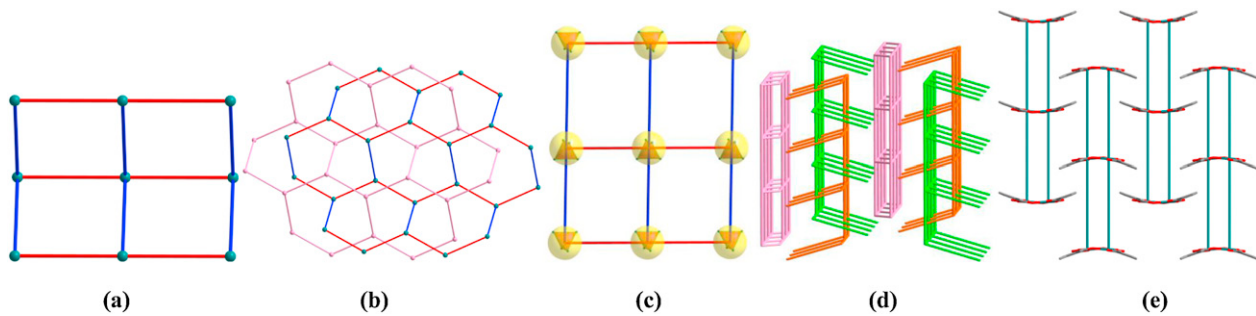
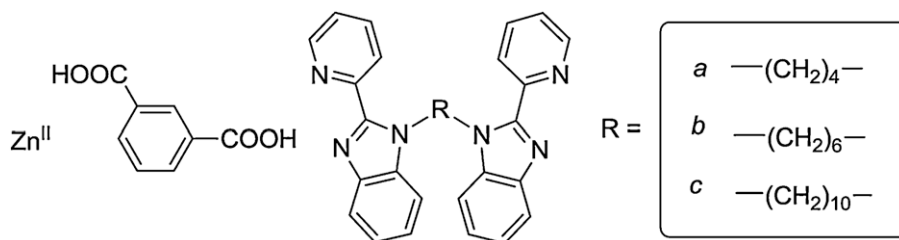


**Fig. 7.** Schematic illustration showing the distinct networks generated from  $\text{Zn}^{\text{II}}$ , ip, and bpy under different reaction conditions: (a) 2D corrugated layers in  $\mathbf{7a}^1$  [70], (b) 2D interpenetrating hcb layers in  $\mathbf{7a}^2$  [70], (c) 2D layer with tetranuclear SBUs bearing  $\text{Zn}_4\text{O}$  cores in  $\mathbf{7a}^3$  [71], (d) two distinct 2D motifs that are paratactically arranged in an ABCD sequence without interpenetration in  $\mathbf{7a}^4$  [72], and (e) interdigitated 2D layers in  $\mathbf{7a}^5$  [73].



**Scheme 6.** Illustration of the mixed-ligand assembled system with  $\text{Zn}^{\text{II}}$ , H<sub>2</sub>ip, and a series of comparable bis[(pyridyl)benzimidazole] ligands with different spacers, including (a) bbpb, (b) hbpb, and (c) dbpb.

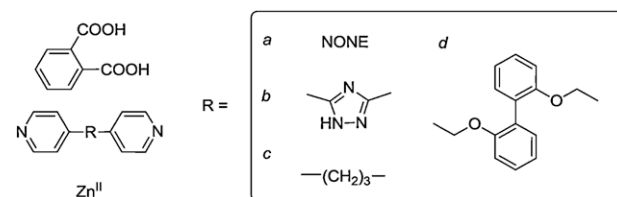
which two types of distinct 2D components are paratactically arranged in an ABCD sequence without interpenetration [72]. By heating the mixture of  $\text{Zn}^{\text{II}}$ , H<sub>2</sub>ip, and bpy in DMF, another 2D layered CP  $\{[\text{Zn}_2(\text{ip})_2(\text{bpy})_2](\text{DMF})\}_n$  ( $\mathbf{7a}^5$ , see Fig. 7e) is formed, which shows the interdigitated porous pattern with a hydrophobic pore surface and selective gas sorption behavior upon structural transformation [73].

By inserting some conjugated spacers between the bipyridine skeleton, such as benzene (for bpib), 1,2,4,5-tetrazine (for bptz), and acetylene (for bpae), three extended bipyridine derivatives can be available to construct microporous CPs (**7b**–**7d**) with  $\text{Zn}^{\text{II}}$  and H<sub>2</sub>ip [74]. Similar to that of  $\mathbf{7a}^5$ , they all show the interdigitated motifs of layers with 1D bottleneck-type channels running along the perpendicular direction of layer stacking, which however possess distinct flexibility owing to the different spacers of the bipyridine bridges. Further, when the intercalary spacers are replaced with flexible ethyl (for bpea) or propyl (for bpp) groups, the resulting coordination networks will be self-adaptable to show entangled features. For example, assembly of  $\text{Zn}^{\text{II}}$ , H<sub>2</sub>ip, and bpea with proper solvents as guests affords a series of CPs  $\{[\text{Zn}(\text{ip})(\text{bpea})]\cdot(\text{guest})\}_n$  with two types of isomeric supramolecular architectures: a 2D rectangular coordination grid interpenetrated by noncovalent (6,3) network consisting of organic guests (**7e**<sup>1</sup>), and a 3D dia polymeric structure of 3-fold interpenetration (**7e**<sup>2</sup>) [75]. However, for  $[\text{Zn}(\text{ip})(\text{bpea})]_n$  (**7e**<sup>3</sup>) with no template solvent, the  $\text{Zn}^{\text{II}}$  ions are extended by the two bridging linkers to afford corrugated sheets with significant voids to be 3-fold interpenetrating [55]. By enlarging the bridging linker from bpea to bpp, the assembled reaction affords a 3D CP  $[\text{Zn}(\text{ip})(\text{bpp})]_n$  (**7f**) with large pores to accommodate 4-fold interpenetration with other sub-lattices [55].

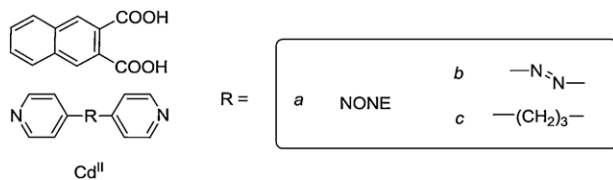
Another typical case for demonstrating the effect of different alkyl spacers of the N-donor ligands on the resulting coordination frameworks can be defined from the reaction system of  $\text{Zn}^{\text{II}}$ , H<sub>2</sub>ip, and the flexible bis[(pyridine)benzimidazole] tectons, namely, bbpb, hbpb, and dbpb (Scheme 6, see a–c). Changing the spacer lengths of such tectons by different  $-(\text{CH}_2)_n-$  groups ( $n=4$ , 6, and 10) will result in drastic changes of flexibility in ligand

binding and linking capability, which thus can well regulate the network structures of CPs from 1D chain motif, to 2D (6,3) sheet pattern, and then to 3D pcu topological architecture of 2-fold interpenetration [76].

In the mixed-ligand assembled system of H<sub>2</sub>pa with two carboxyl groups in a more acute angle, and different bipyridine co-ligands (Scheme 7, see a–d), the significant spacer effect of such tectons on the construction of CPs will further be observed. In  $\{[\text{Zn}(\text{pa})(\text{bpy})(\text{H}_2\text{O})_2](\text{H}_2\text{O})_2\}_n$  (**8a**) [77], both types of ligands play bridging roles to extend the  $\text{Zn}^{\text{II}}$  ions into a regular square-grid polymeric sheet. By inserting the triazolyl spacer between the two pyridine terminals, the longer 4,4'-bpt ligand can be used to react with H<sub>2</sub>pa and  $\text{Zn}^{\text{II}}$  to form a 2D CP  $[\text{Zn}(\text{pa})(4,4'\text{-bpt})]_n$  (**8b**) with a wave-like layered motif [51], being more distorted in comparison with **8a**. Relying on the relative orientation of three methylene groups between the pyridine groups, the flexible bpp ligand can adopt distinct conformations in coordination assemblies. In  $\{[\text{Zn}_2(\text{pa})_2(\text{bpp})_2](\text{H}_2\text{O})_2\}_n$  (**8c**) [78], the phthalate-bridged helical arrays  $[\text{Zn}(\text{pa})]_n$  are interlinked by bpp linkers with different conformations to form a 3D acentric CP with cds topology. When replaced with a more bulky substituent between the two pyridine terminals, the resulting flexible bpmbp tecton can be assembled with H<sub>2</sub>pa and  $\text{Zn}^{\text{II}}$  ions to form  $[\text{Zn}(\text{pa})(\text{bpmbp})]_n$  (**8d**) showing a 1D two-leg ladder motif [79], in which the  $[\text{Zn}(\text{bpmbp})]_n$  chains can be considered as the side rails and pa<sup>2+</sup> ligands as the cross rungs.



**Scheme 7.** Illustration of the mixed-ligand assembled system with  $\text{Zn}^{\text{II}}$ , H<sub>2</sub>pa, and a series of comparable bipyridyl ligands with different spacers, including (a) bpy, (b) 4,4'-bpt, (c) bpp, and (d) bpmbp.



**Scheme 8.** Illustration of the mixed-ligand assembled system with Cd<sup>II</sup>, 2,3-H<sub>2</sub>ndc, and a series of comparable bipyridyl ligands with different spacers, including (a) bpy, (b) azpy, and (c) bpp.

As an analogue but bulkier derivative of H<sub>2</sub>pa, 2,3-H<sub>2</sub>ndc with the extended  $\pi$ -conjugated skeleton has also been utilized to assemble with Cd<sup>II</sup> and comparable bpy-like bridging tectons (**Scheme 8**, see *a–c*), yielding a series of CPs to demonstrate the spacer effect [80]. With regard to  $\{[\text{Cd}(2,3\text{-ndc})(\text{bpy})_{0.5}(\text{H}_2\text{O})_2](\text{H}_2\text{O})\}_n$  (**9a**), the Cd<sup>II</sup> centers are extended by 2,3-ndc and bpy along two different axes to form a 2D coordination layer of (3,4)-connected (4<sup>2</sup>.6)(4<sup>2</sup>.6<sup>3</sup>.8) pattern (see Fig. 8a). In order to explore further the effect of spacers on the molecular tectonics of CPs, a semi-rigid ligand azpy with rich  $\pi$ -conjugated backbone is used to construct a 3D mixed-ligand CP  $\{[\text{Cd}(2,3\text{-ndc})(\text{azpy})(\text{H}_2\text{O})](\text{H}_2\text{O})\}_n$  (**9b**) (see Fig. 8b). The final architecture can be simplified as an unusual uninodal 4-connected **irl** net with (4<sup>2</sup>.6<sup>3</sup>.8) topology. When the more flexible bpp co-ligand with the separation of two coordination sites of ca. 10 Å is used, a 3D chiral CP  $\{[\text{Cd}(2,3\text{-ndc})(\text{bpp})_2](\text{H}_2\text{O})_3\}_n$  (**9c**) can be obtained (see Fig. 8c). Within this structure, a pair of right-handed and left-handed 2<sub>1</sub> helical chains of  $[-\text{Cd--bpp--}]_n$  and  $[-\text{Cd--(2,3-ndc)--}]_n$ , running perpendicularly along the [100] and [010] axes, respectively, are extended by Cd–O/N coordination bonds to afford a 3D **dia** lattice. A remarkable spacer effect has also been observed with the homologous mixed-ligand CP systems of Ag<sup>I</sup> and Zn<sup>II</sup> metal centers [81].

By comparison, selecting those aromatic dicarboxylic acids with flexible spacers will bring more intricacy into CPs. In this context, the mixed-ligand assembled system of H<sub>2</sub>oba and the bipyridine-type co-ligands (**Scheme 9**, see *a–d*) is a representative example to demonstrate the spacer effect therein. Owing to the oxygen center positioning between the two benzenecarboxyl groups, the adjustable connecting angle C<sub>carboxyl</sub>–O–C<sub>carboxyl</sub> of H<sub>2</sub>oba will be responsive to the diverse CP structures. Notably, assembly of Zn<sup>II</sup> with bpy and the flexible H<sub>2</sub>oba ligand gives three distinct CPs under different conditions. In  $[\text{Zn}_2(\text{oba})_2(\text{bpy})]_n$  (**10a**<sup>1</sup>) [82], the trigonal-bipyramidal Zn<sup>II</sup> ions are connected by the mixed ligands to constitute a 3D CP (see Fig. 9a), where the oba ligands exhibit two different connecting angles (116 and 125°). In  $\{[\text{Zn}_2(\text{oba})_2(\text{bpy})](\text{DMA})\}_n$  (**10a**<sup>2</sup>) [83], the angular connector oba (118°) with the aid of bpy, can interlink the paddle-wheel binuclear  $[\text{Zn}_2(\text{COO})_4]$  SBUs into a 3D CP (see Fig. 9b), which interestingly exhibits an unique selectivity for the detection of high explosives and other aromatics via fluorescence quenching and enhancement mechanism. With respect to CP  $\{[\text{Zn}_3(\mu_3\text{-OH})(\mu_2\text{-OH})(\text{bpy})_{0.5}(\text{oba})_2](\text{H}_2\text{O})_{0.5}\}_n$  (**10a**<sup>3</sup>) [84], the trimeric  $[\text{Zn}_3(\mu_3\text{-OH})]$  cores are extended by  $\mu_2\text{-OH}$  groups to produce unprecedented helical chains, which are pillared by bpy and oba (124 and 116°) to afford a 3D network (see Fig. 9c). Assembly of H<sub>2</sub>oba with Zn<sup>II</sup> and bptz co-ligand yields a 3D self-catenated framework  $\{[\text{Zn}_2(\text{oba})_2(\text{bptz})](\text{DMF})_2\}_n$  (**10b**), exhibiting a uninodal 6-connected network with (4<sup>4</sup>.6<sup>10</sup>.8) topology (see Fig. 9d) that can be properly attributed to the mixed-linkers of angular oba (117°) and elongated pytz [85]. Further introduction of the –N=N– and –C=C– spacers [86] into the bipyridine ligands will lead to more structural diversity. In  $\{[\text{Zn}_2(\text{oba})_2(\text{azpy})(\text{DMF})_2](\text{DMF})_6\}_n$  (**10c**) [87], the oba (122°) and azpy ligands play the roles of side rails and rungs, respectively, linking the Zn<sup>II</sup> ions to form a 1D ladder (see Fig. 9e). For  $\{[\text{Zn}_2(\text{oba})_2(\text{bpee})](\text{DMF})_2(\text{H}_2\text{O})_4\}_n$  (**10d**) [87],

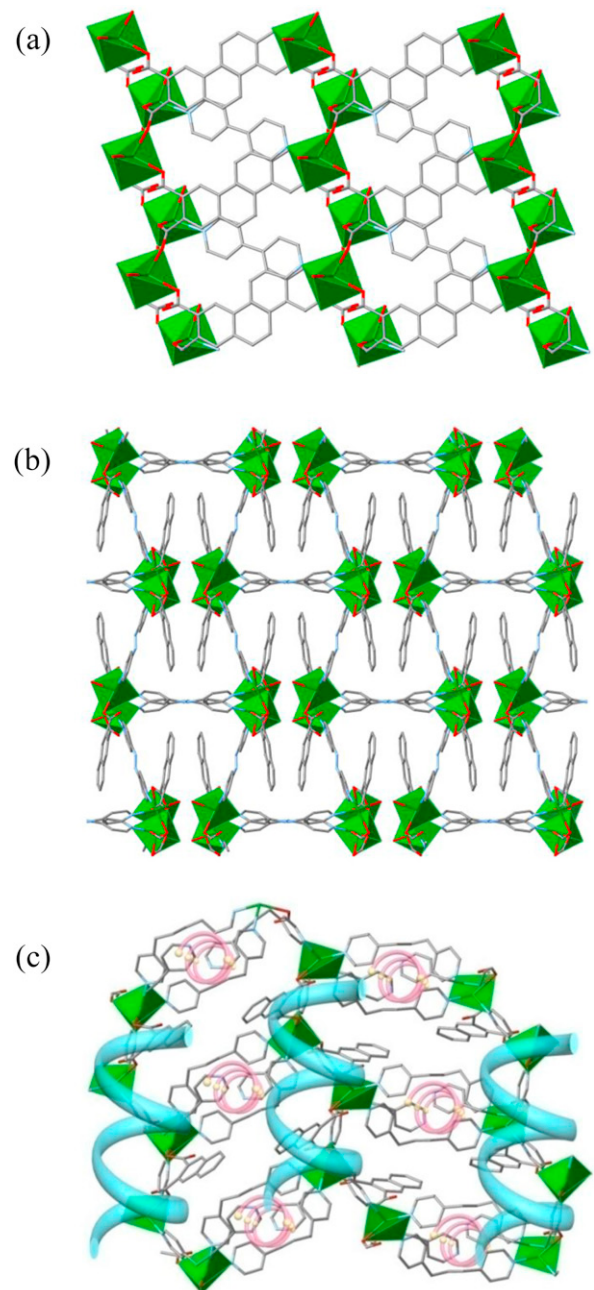
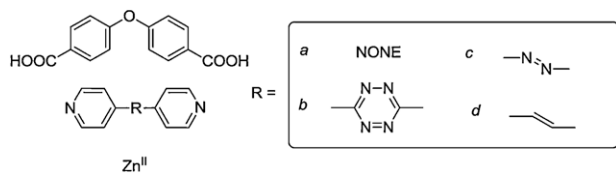


**Fig. 8.** Packing diagrams of the CPs combining Cd<sup>II</sup>, 2,3-ndc, and a family of bipyridine co-ligands: bpy, azpy, and bpp [80]. (a) 2D coordination layer of (3,4)-connected network in **9a**. (b) 3D uninodal 4-connected **irl** net in **9b**. (c) 3D **dia** lattice with different helical chains along the perpendicular directions in **9c**.

the distorted oba ligands (125°) with a more obtuse angle connect the Zn<sup>II</sup> centers to form a 2D sheet with  $[\text{Zn}_2(\text{COO})_4]$  paddle-wheel SBUs, which are further pillared by the bpee linkers to construct a 3D coordination network (see Fig. 9f).



**Scheme 9.** Illustration of the mixed-ligand assembled system with Zn<sup>II</sup>, H<sub>2</sub>oba, and a series of comparable bipyridyl ligands with different spacers, including (a) bpy, (b) pytz, (c) azpy, and (d) bpee.

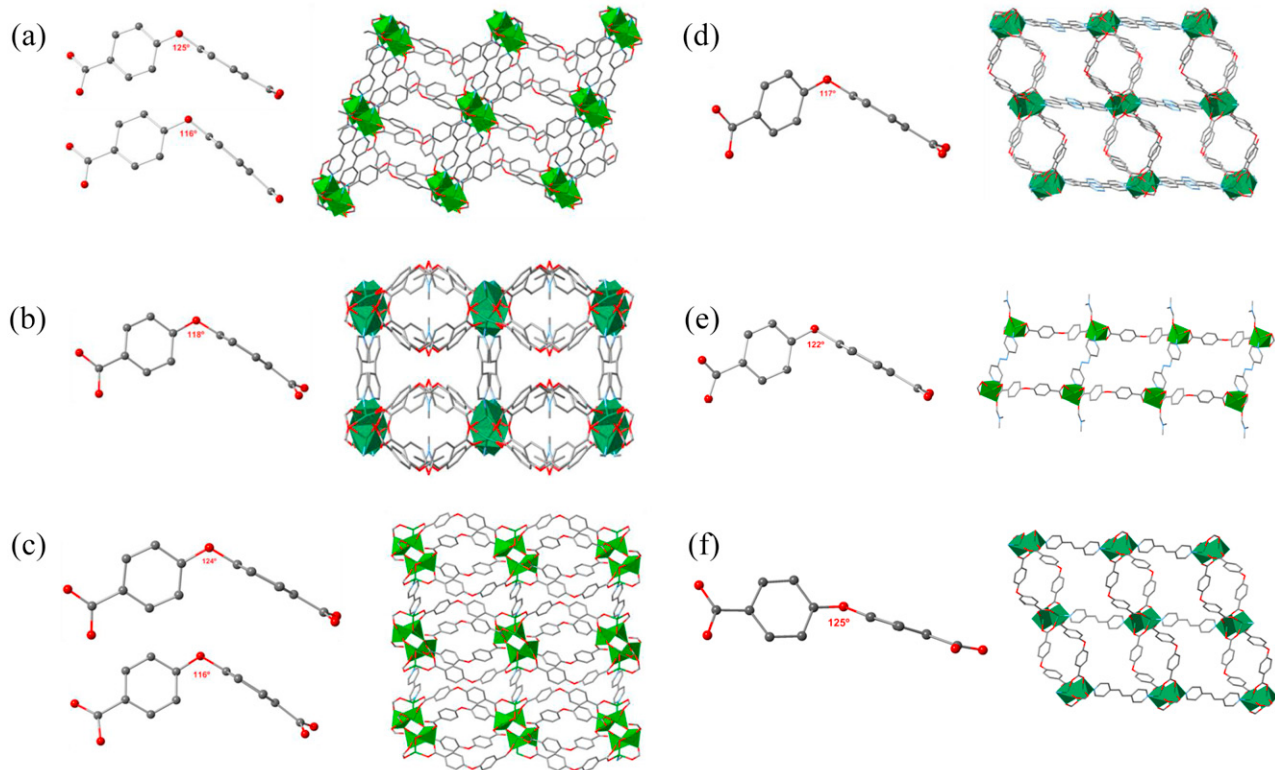


**Fig. 9.** (a–c) Distinct 3D networks generated from  $Zn^{II}$ , oba, and bpy under different reaction conditions in **10a<sup>1</sup>**–**10a<sup>3</sup>**, showing the trigonal-bipyramidal  $[ZnO_3N_2]$ , binuclear paddle-wheel  $[Zn_2(COO)_4]$ , and trinuclear  $[Zn_3(\mu_3-OH)]$  SBUs, respectively [82–84]. (d) 3D network of  $\{[Zn_2(oba)_2(pytz)](DMF)_2\}_n$  (**10b**) [85]. (e) 1D ladder structure of  $\{[Zn_2(oba)_2(azpy)](DMF)_2\}(DMF)_6\}_n$  (**10c**) [87]. (f) 3D pillared-layer structure of  $\{[Zn_2(oba)_2(bpee)](DMF)_2(H_2O)_4\}_n$  (**10d**) [87]. The tortuous oba ligands are also shown with the distortion angles.

Very recently, Wang et al. have developed a family of mixed-ligand CPs on the basis of a multicarboxylate ligand  $H_3nbtc$  and different bipyridine-type co-ligands (Scheme 10, see *a*–*d*). Reactions of  $Zn^{II}$  with  $H_3nbtc$  and bpy or bpee produce two unusual 3D self-penetrating CPs of 4-connected  $(4.10^4.12)_2(4^3.6^2.8)_2(4^4.6^2)$  and  $(4.6^2.7^2.8)_2(4^2.6^2.7.8)$  topologies, respectively [88]. Replacing the spacers of bipyridine co-ligands by ethyl (bpea) or propyl (bp), another two 3D  $Zn^{II}$  CPs showing a trinodal (4,5)-connected  $(3.4.5^3.6)(3.5^2.6^2.8^4.9)(3.4.5.8^3)$  and a 4-connected  $(4.6^4.8)(4^4.6^2)(4^3.6^3)$  topological networks are afforded, respectively [89]. Owing to the distinct spacers within the bipyridine co-ligands, the resulting 3D coordination frameworks can be modulated from the self-entangled to normal networks with different topologies. Similarly, the significant spacer effect has also been demonstrated in the  $Cd^{II}$  [89],  $Mn^{II}$  [90],  $Co^{II}$  [91],  $Cu^{II}$  [91], and  $Ni^{II}$  [91] CPs with such mixed ligands.

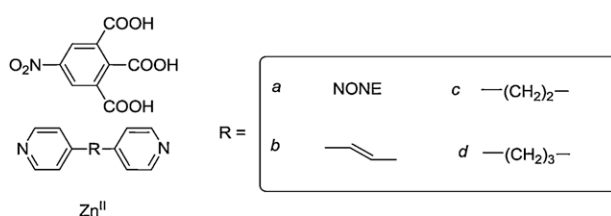
In general, enhancement of the ligand lengths may cause the framework interpenetration of CPs to decrease the void volumes of overall crystal lattices. However, Cao et al. have reported a series of non-interpenetrating CPs formulated as  $\{[Cd_4(tdpm)L_4](solvent)\}_n$

( $L = bpy$  for **11a**;  $azpy$  for **11b**;  $bpea$  for **11c**;  $bp$  for **11d**, Scheme 11, see *a*–*d*) based on the pillaring strategy of mixed-ligand systems. Significant spacer effect has been observed, that is, the pore sizes can be continuously tuned with elongation of the pillars and the network topologies vary from **nbo** to **mot** types for different stacking fashions of the layers [92]. In these four CPs, the binuclear  $[Cd_2(\mu-O)_2O_6N_4]$  metal clusters are connected by mix-pillared building blocks, in which one of them is varied by length and flexibility to result in different pore sizes and network topologies. In **11a**–**11c**, the architectures show the **nbo** topology with the window dimensions of the network cavities ranging from  $11.7 \times 10.0$  to  $14.0 \times 10.0 \text{ \AA}^2$  (see Fig. 10a–c). Notably, due to the different dispositions of the layers along the *c* axis, **11d** takes a distinct **mot** network with the pore size of  $16.1 \times 10.0 \text{ \AA}^2$  (see Fig. 10d).

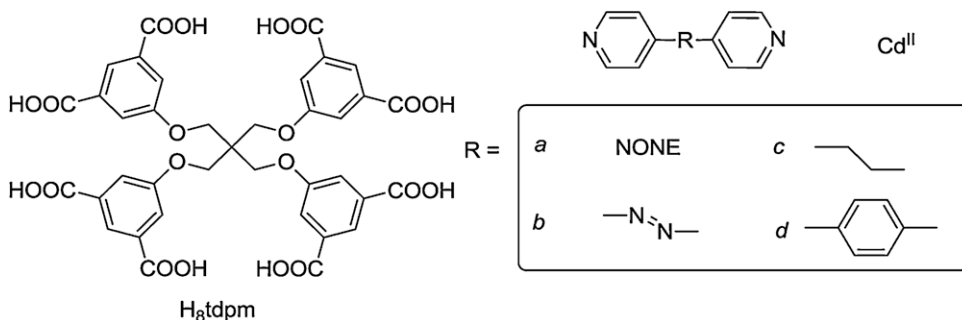
### 2.3.2. Positional isomeric effect

Ligands with the same coordination groups but locating at different positions may lead to significant positional isomerism to affect the structural assemblies of CPs, especially for mixed-ligand CP systems.

As the most representative examples of positional isomerism, the three aromatic dicarboxylic acids ( $H_2pa$ ,  $H_2ip$ , and  $H_2tp$ ), possessing an angle-increased binding tendency, are active in regulating the structural assemblies of mixed-ligand CPs (Scheme 12, see *a*–*c*). Reactions of bpy and  $Cd^{II}$  with this series of isomeric dicarboxyl ligands result in diverse structures. In  $[Cd(Hpa)_2(bpy)]_n$  (**12a**), the  $Cd^{II}$  centers are bridged by the V-shaped Hpa ligands to produce exclusive right-handed helical chains, which are further extended by bpy to afford a fascinating 3D chiral network [93]. When  $H_2pa$  is replaced with  $H_2ip$ , the resulting  $\{[Cd(ip)(bpy)](H_2O)\}_n$  (**12b**) shows a 2D rectangular grid-like layer via the interlinking roles of ip and bpy along different



**Scheme 10.** Illustration of the mixed-ligand assembled system with  $Zn^{II}$ ,  $H_3nbtc$ , and a series of comparable bipyridyl ligands with different spacers, including (a) bpy, (b) bpea, (c) bpea, and (d) bp.



**Scheme 11.** Illustration of the mixed-ligand assembled system with  $\text{Cd}^{\text{II}}$ ,  $\text{H}_8\text{tdpm}$ , and a series of comparable bipyridyl ligands with different spacers, including (a) bpy, (b) azpy, (c) bpea, and (d) bpb.

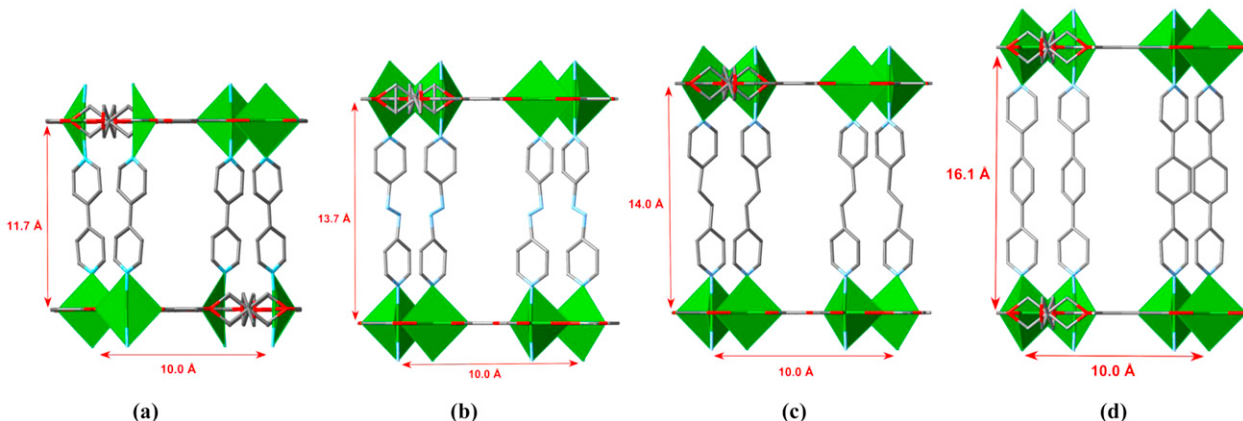
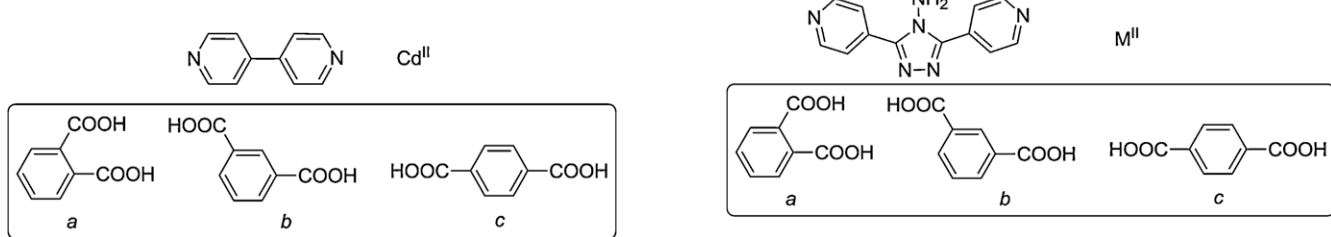


**Fig. 10.** Schematic illustration showing the cubic frameworks with different pillars: (a) bpy, (b) azpy, (c) bpea, and (d) bpb [92].

directions [94]. Solvothermal reactions of  $\text{Cd}^{\text{II}}$ , bpy, and  $\text{H}_2\text{tp}$  can afford two distinct CPs, a non-interpenetrating 3D **pcu** framework  $\{[\text{Cd}(\text{tp})(\text{bpy})](\text{DMF})_3(\text{H}_2\text{O})\}_n$  (**12c<sup>1</sup>**) and its 2-fold interpenetrating form  $[\text{Cd}(\text{tp})(\text{bpy})]_n$  (**12c<sup>2</sup>**), which can be easily synthesized with good phase purity by changing the reaction temperature and the concentration of starting materials [50,95]. Specifically, lower temperature and concentration will favor the isolation of **12c<sup>1</sup>**, while increasing both such parameters leads to the formation of **12c<sup>2</sup>**.

Recently, some analogous linkers derived from the proper modification of the classical bpy tecton have been employed in coordination assemblies, which have dissimilar backbone flexibility and thus, give rise to a profound steric effect on the direction of unexpected coordination motifs. In this regard, mixed-ligand CPs with a bent bipyridine derivative 4,4'-abpt and isomeric dicarboxylates (Scheme 13, see *a*–*c*) can be modulated by such positional isomeric tectons. For example, a series of mixed-ligand  $\text{Cd}^{\text{II}}$  CPs have been synthesized by the combination of 4,4'-abpt and the benzenedicarboxylate isomers  $\text{H}_2\text{pa}$ ,  $\text{H}_2\text{ip}$ , and  $\text{H}_2\text{tp}$  [96,97]. Their structural analysis reveals that these isomers

show versatile interconnecting functions to manage the metal centers to form various coordination networks. For  $\{[\text{Cd}(4,4'\text{-abpt})(\text{pa})(\text{H}_2\text{O})]\}(\text{H}_2\text{O})_n$  (**13a**), the neighboring  $\text{Cd}^{\text{II}}$  ions are connected by the pa components to produce 1D polymeric chains along the [010] direction, which are further extended via the 4,4'-abpt spacers to result in a 2D (4,4) layer (see Fig. 11a). In  $\{[\text{Cd}_2(4,4'\text{-abpt})(\text{ip})_2(\text{H}_2\text{O})_4](\text{H}_2\text{O})_6\}_n$  (**13b**), each  $\text{Cd}^{\text{II}}$  center can be regarded as a 3-connected T-shaped connector, and is surrounded by the carboxylate oxygen donors of two ip ligands in the horizontal orientation and a bipyridine nitrogen atom in the vertical direction. Thus, the extension of such T-shaped  $\text{Cd}^{\text{II}}$  nodes gives a 2D bilayer with (8<sup>2</sup>.10) topology. Notably, the bilayer arrays exhibit a unique structural feature of 3D stacking, which are alternately arranged in tongue-and-groove interpenetrating mode and interdigitating fashion (see Fig. 11b). The coordination networks of  $\{[\text{Cd}(4,4'\text{-abpt})(\text{tp})(\text{H}_2\text{O})_2](\text{DMF})_{1.5}(\text{H}_2\text{O})\}_n$  (**13c<sup>1</sup>**) and  $\{[\text{Cd}_2(4,4'\text{-abpt})_2(\text{tp})_2(\text{H}_2\text{O})(\text{DMF})]\}(\text{DMF})_2\}_n$  (**13c<sup>2</sup>**) seem similar although they crystallize in different space groups ( $P2_1/n$  vs  $P\bar{1}$ ), which exhibit the 2D corrugated layers of 2-fold interpenetrating



**Scheme 12.** Illustration of the mixed-ligand assembled system with  $\text{Cd}^{\text{II}}$ , bpy, and three isomeric aromatic dicarboxylic acids, including (a)  $\text{H}_2\text{pa}$ , (b)  $\text{H}_2\text{ip}$ , and (c)  $\text{H}_2\text{tp}$ .

**Scheme 13.** Illustration of the mixed-ligand assembled system with  $\text{M}^{\text{II}}$  ( $\text{Cd}^{\text{II}}$  or  $\text{Co}^{\text{II}}$ ), 4,4'-abpt, and three isomeric aromatic dicarboxylic acids, including (a)  $\text{H}_2\text{pa}$ , (b)  $\text{H}_2\text{ip}$ , and (c)  $\text{H}_2\text{tp}$ .

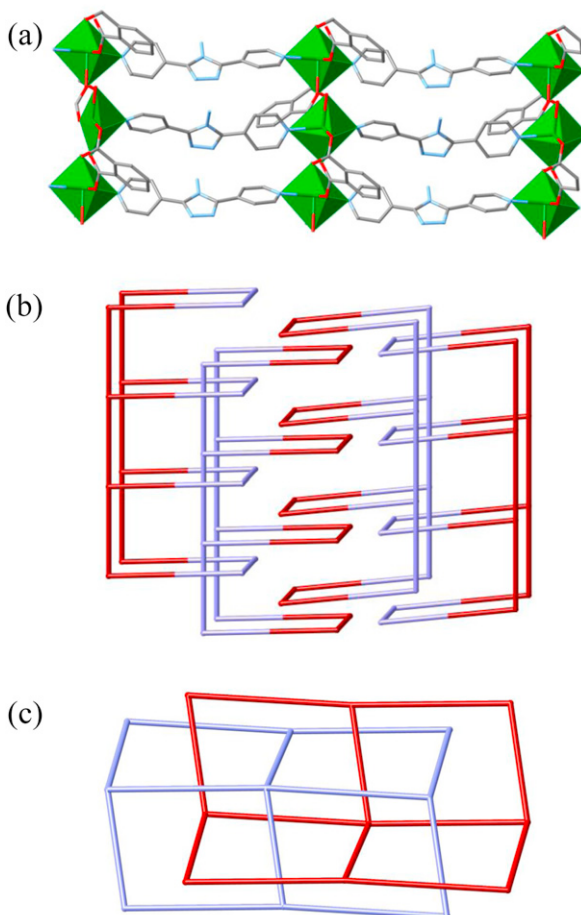
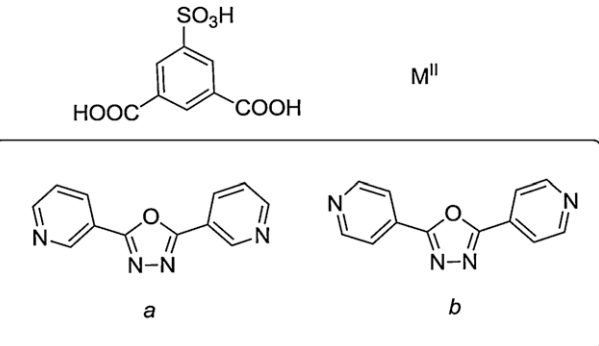


**Fig. 11.** (a) 2D (4,4) layer in  $\{[Cd(4,4'\text{-abpt})(pa)(H_2O)](H_2O)\}_n$  (**13a**) [96]. (b) 2D bilayer motif with  $(8^2.10)$  network topology in  $\{[Cd_2(4,4'\text{-abpt})(ip)_2(H_2O)_4](H_2O)_6\}_n$  (**13b**) showing the tongue-and-groove interpenetrating mode and interdigitating fashion [96]. (c) 2D corrugated layers in  $\{[Cd(4,4'\text{-abpt})_2(tp)(H_2O)_2](DMF)_{1.5}(H_2O)\}_n$  (**13c<sup>1</sup>**) and  $\{[Cd_2(4,4'\text{-abpt})_2(tp)_2(H_2O)(DMF)](DMF)_2\}_n$  (**13c<sup>2</sup>**) of 2-fold interpenetrating mode [96,97].

mode, resulting from the linkages of both tp and 4,4'-abpt bridging ligands (see Fig. 11c). Additionally, a similar isomeric effect has been observed in the corresponding Co<sup>II</sup> CP system [96].

By considering the flexibility of organic ligands, such a structure-directing effect of the orientation of carboxyl groups will be more evident in CP assembly. For example, combining the flexible bix ligand and Cd<sup>II</sup> with a series of flexible isomers of phenylenediacetic acids (*o*/*m*/*p*-H<sub>2</sub>pda, Scheme 14, see *a*–*c*) will lead to the formation of three distinct CPs [98]. In the 2D nets of  $[Cd(o\text{-pda})(bix)]_n$  (**14a**) and  $[Cd(m\text{-pda})(bix)_{0.5}(H_2O)]_n$  (**14b**), hetero-handed helical arrays are constructed due to the ligand flexibility, which exhibit a (3,5)-connected  $(4^2.6)(4^2.6^7.8)$  topology and a (3,4)-connected

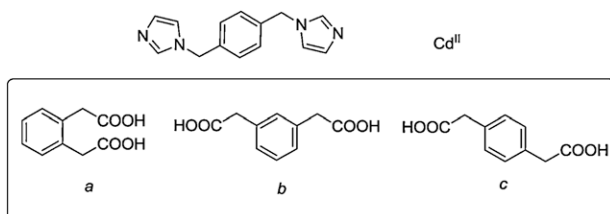


**Scheme 15.** Illustration of the mixed-ligand assembled system with M<sup>II</sup> (Cd<sup>II</sup> or Co<sup>II</sup>), H<sub>3</sub>sip, and a pair of isomeric bipyridyl derivatives, including (a) 3-bpo and (b) 4-bpo.

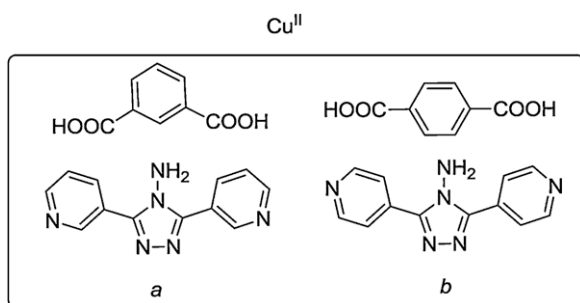
V<sub>2</sub>O<sub>5</sub>-type  $(4^2.6)(4^2.6^3.8)$  topology, respectively. In contrast, CP  $[Cd(p\text{-pda})(bix)]_n$  (**14c**) shows a distinct 3D **dia** framework of 5-fold interpenetration.

As stated above, modifying the positions of carboxyl groups on aromatic ligand backbones represents an effective approach to regulate the CP crystal structures. To further explore the isomeric effect of bipyridine ligands on CP structural assemblies, a bent bipyridine derivative 4-bpo and its 3-N-donor isomer 3-bpo with versatile binding fashions are selected (Scheme 15, see *a*–*b*). The diversity of the established structural motifs constructed by two such building blocks and familiar metal ions has been reviewed [99], which illustrates the broad range of the resulting coordination architectures [99,100]. In comparison with the simple bipyridine ligands, there are several interesting features of 3-bpo and 4-bpo tectons as described below. (a) Both ligands with multiple coordination sites can adopt different binding fashions to construct diverse coordination patterns. (b) Their ligand geometries are bent and variable. That is, the dihedral angles between the oxadiazole group and two terminal pyridine groups as well as the angle between the centroid of oxadiazole and two pyridine nitrogen donors are adaptable to meet the coordination requirements. (c) The oxadiazole ring usually has a tendency to completely or partly participate in secondary interactions, through which the resulting lattice arrangements of coordination motifs may be significantly influenced. (d) Especially, the 3-bpo ligand can potentially adopt three typical conformations to self-adjust in coordination assemblies. For example, reactions of Cd<sup>II</sup> with H<sub>3</sub>sip and 3-bpo or 4-bpo under acidic condition (pH 2.5) produce two distinct CPs [21]. Owing to the different coordination modes and conformations of the mixed ligands, the resulting network structures present the 2D polymeric layer and 1D zigzag chain patterns. In a similar way, reactions of Co<sup>II</sup> with H<sub>3</sub>sip and 3-bpo or 4-bpo afford a discrete coordination complex or a 1D array, respectively, manipulated by the positional isomeric character of the ligands [21]. In this regard, Yan et al. have also systematically studied the impact of positional isomeric ligands on the structures and magnetic properties of Co<sup>II</sup> CPs with three bipyridine tectons bearing 1*H*-1,2,4-triazole spacer (4,4'-, 3,4'- and 3,3'-bpt) and phenyl dicarboxylates, which display a variety of network structures and different magnetic behaviors [101].

Altering both the acid- and base-type positional isomeric tectons in a CP assembly will result in more significant structural divergence. For example, similar reactions of Cu<sup>II</sup> salt with mixed-ligand system 3,3'-abpt/H<sub>2</sub>ip or 4,4'-abpt/H<sub>2</sub>tp (Scheme 16, see *a*–*b*) afford two CPs. In  $\{[Cu(ip)(3,3'\text{-abpt})](H_2O)_2\}_n$  (**15a**), the bent ip ligands link the Cu<sup>II</sup> ions to result in 1D ribbons along [010], which are further extended through the bent 3,3'-abpt bridges to afford a 2D (4,4) net (see Fig. 12a) [102]. However, CP  $\{[Cu(tp)(4,4'\text{-abpt})(H_2O)]_2[Cu(tp)(4,4'\text{-abpt})_2](H_2O)_2\}_n$  (**15b**) that involves the



**Scheme 14.** Illustration of the mixed-ligand assembled system with Cd<sup>II</sup>, bix, and three isomeric phenylenediacetic acids, including (a) *o*-H<sub>2</sub>pda, (b) *m*-H<sub>2</sub>pda, and (c) *p*-H<sub>2</sub>pda.

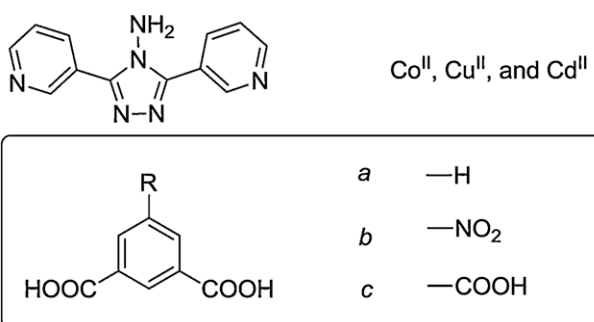


**Scheme 16.** Illustration of the mixed-ligand assembled system with  $\text{Cu}^{\text{II}}$  and (a) 3,3'-abpt/H<sub>2</sub>ip or (b) 4,4'-abpt/H<sub>2</sub>tp.

more linear linkers tp and 4,4'-abpt consists of two distinct polymeric motifs: an infinite tp-bridged 1D array and a planar 2D (4,4) net generated from the connectivity of both tp and 4,4'-abpt bridges, which are further entangled to construct a unique 1D + 2D → 3D polythreading architecture (see Fig. 12b) [97]. Similar results are also found in the  $\text{Ni}^{\text{II}}$  CPs involving the mixed-ligand system 3,3'-abpt/tp [103] or 4,4'-abpt/tp [96], showing a 1D chain and a 2D square grid layer, respectively.

### 2.3.3. Substituent effect

Theoretically speaking, the substituents attached to the backbones of organic ligands probably influence the network structures of CPs in two aspects [104–107]. On the one hand, they may possess additional interconnecting functions to extend the coordination



**Scheme 17.** Illustration of the mixed-ligand assembled system with  $\text{Co}^{\text{II}}/\text{Cu}^{\text{II}}/\text{Cd}^{\text{II}}$ , 3,3'-abpt, and a series of comparable *R*-isophthalic acids with different substituents, including (a) H<sub>2</sub>ip, (b) H<sub>2</sub>nip, and (c) H<sub>3</sub>tma.

motifs, in view of their ability to form coordination and secondary interactions such as H-bonding and aromatic stacking. On the other hand, those inert substituents may impose remarkable steric and/or electronic effects on the binding properties of organic ligands, and consequently, the network structures of the resulting CPs.

A series of  $\text{Co}^{\text{II}}$ ,  $\text{Cu}^{\text{II}}$  or  $\text{Cd}^{\text{II}}$  CPs have been constructed by selecting 3,3'-abpt incorporated with H<sub>2</sub>ip, H<sub>2</sub>nip, and H<sub>3</sub>tma, respectively, as building blocks (Scheme 17, see a–c) [102]. For instance,  $\{[\text{Cd}(\text{ip})(3,3'\text{-abpt})(\text{H}_2\text{O})](\text{H}_2\text{O})_{1.5}\}_n$  (**16a**) shows a 1D molecular ladder array, where the mixed ligands 3,3'-abpt and ip serve as the rung and railway, respectively (see Fig. 13a). In comparison, although the nitro group in H<sub>2</sub>nip is seldom engaged in metal coordination, it will significantly change the electronic density of the ligand as a strong electron withdrawing group, and also can be regarded as a reliable hydrogen-bonding acceptor. With this understanding, the 2D (6,3) coordination layers in  $\{[\text{Cd}_2(\text{nip})_2(3,3'\text{-abpt})_2(\text{H}_2\text{O})_4](\text{H}_2\text{O})_2\}_n$  (**16b**) (see Fig. 13b) are further extended by the nitro-involved H-bonding interactions to afford a 3D network. The 5-carboxyl group of H<sub>3</sub>tma can be presented as the potential deprotonation regulator, active coordination site, and donor/acceptor of H-bonding. As a result, in the 1D chain-like CP  $\{[\text{Cd}(\text{Htma})(3,3'\text{-abpt})(\text{H}_2\text{O})_2](\text{H}_2\text{O})_2\}_n$  (**16c**) (see Fig. 13c), the Htma ligand takes the dianion form for charge balance with 5-carboxyl and as the H-bonding donor for lattice extension.

A series of  $\text{Cd}^{\text{II}}$  CPs have been designed and hydrothermally synthesized using 3-bpo and *R*-isophthalic acids ( $R = -\text{H}$ , H<sub>2</sub>ip;  $-\text{CH}_3$ , H<sub>2</sub>mip;  $-\text{OCH}_3$ , H<sub>2</sub>moip;  $-\text{tBu}$ , H<sub>2</sub>tbip;  $-\text{OH}$ , H<sub>2</sub>hip;  $-\text{NO}_2$ , H<sub>2</sub>nip), which show diverse 1D and 2D coordination networks [108]. The substituent effect of *R*-isophthalate and the adaptable conformations of 3-bpo (*cisoid-I*, *cisoid-II*, and *transoid*) play a decisive role in directing the assembly of such mixed-ligand CPs (Scheme 18, see a–f). In  $\{[\text{Cd}_2(\text{ip})_2(3\text{-bpo})_2(\text{H}_2\text{O})_2](\text{H}_2\text{O})_2\}_n$  (**17a**) and  $[\text{Cd}(\text{mip})(3\text{-bpo})]_n$  (**17b**), all the 3-bpo ligands adopt the *cisoid-I* conformation, which connect the  $\text{Cd}^{\text{II}}$  ions with the aid of bridging *R*-isophthalates to form a 1D double chain and a 1D cage-like array, respectively (see Fig. 14a and b). In the structure of  $[\text{Cd}_2(\text{moip})_2(3\text{-bpo})_2(\text{H}_2\text{O})_3](\text{H}_2\text{O})_3$  (**17c**), there are two types of 2D coordination nets, in which the moip ligands show the bis-chelating connecting fashion and the 3-bpo ligands take the *cisoid-I* and *cisoid-II* conformations with different unidentate and bridging coordination modes (see Fig. 14c). Interestingly, due to the difference of two such sets of 2D layers that are arranged in the ABAB way with polythreading character, the overall crystal displays chiral nature (see Fig. 14c). When H<sub>2</sub>tbip and H<sub>2</sub>ip are employed, a pair of comparable 2D CPs  $[\text{Cd}_2(\text{tbip})_2(3\text{-bpo})(\text{H}_2\text{O})_4]_n$  (**17d**) and  $[\text{Cd}_2(\text{hip})_2(3\text{-bpo})_3(\text{H}_2\text{O})_2](\text{H}_2\text{O})_8$  (**17e**) are obtained, in which the 3-bpo ligands present the *cisoid-II* and *transoid* conformations, respectively (see Fig. 14d and e). When H<sub>2</sub>nip with the electron-withdrawing substituent is used instead, a 1D CP  $\{[\text{Cd}(\text{nip})(3\text{-bpo})](\text{H}_2\text{O})\}_n$  (**17f**) that is similar to **17b** is achieved

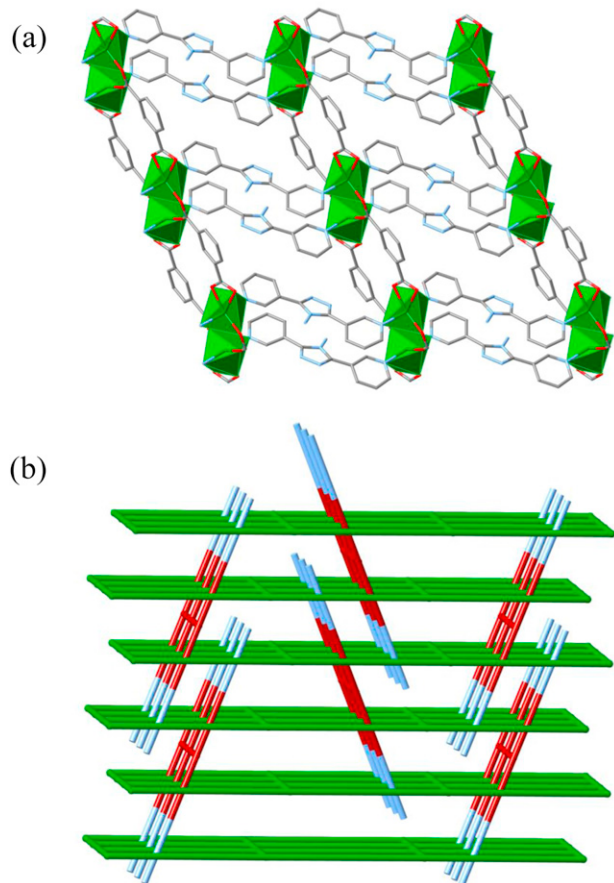


**Fig. 12.** Two  $\text{Cu}^{\text{II}}$  CPs combining mixed ligands (a) 3,3'-abpt/ip and (b) 4,4'-abpt/tp, showing 2D (4,4) network (**15a**) [102] and 1D+2D→3D polythreaded architecture (**15b**) [97], respectively.

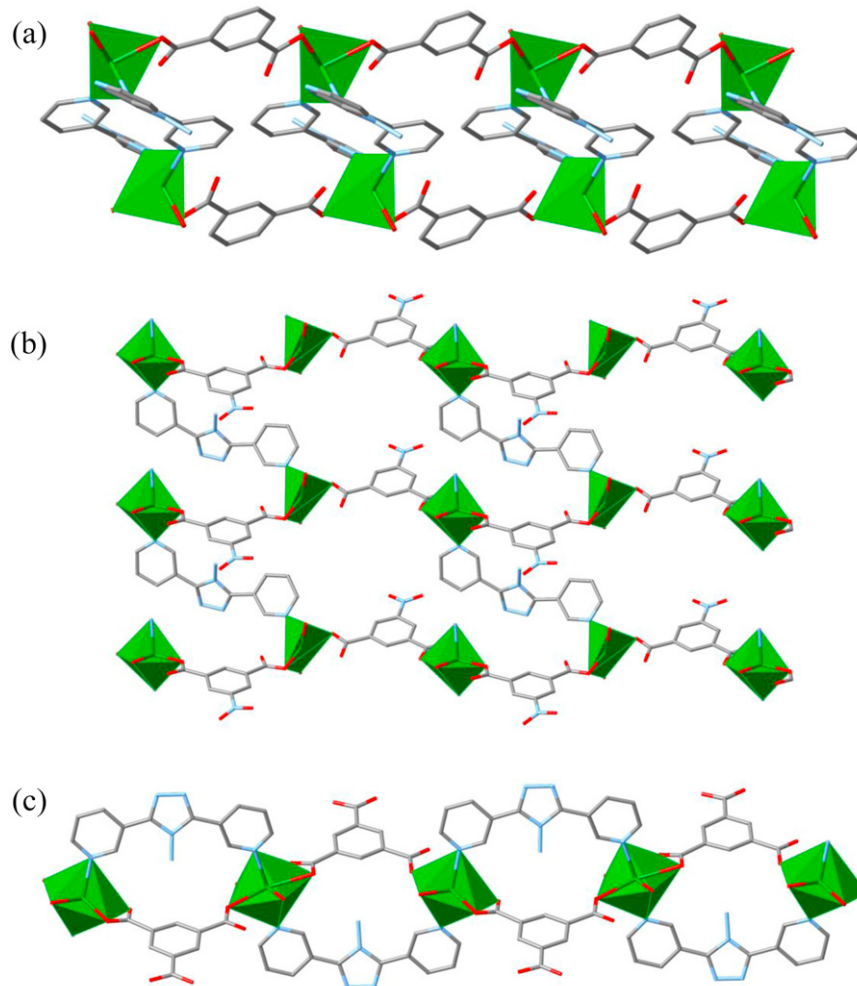
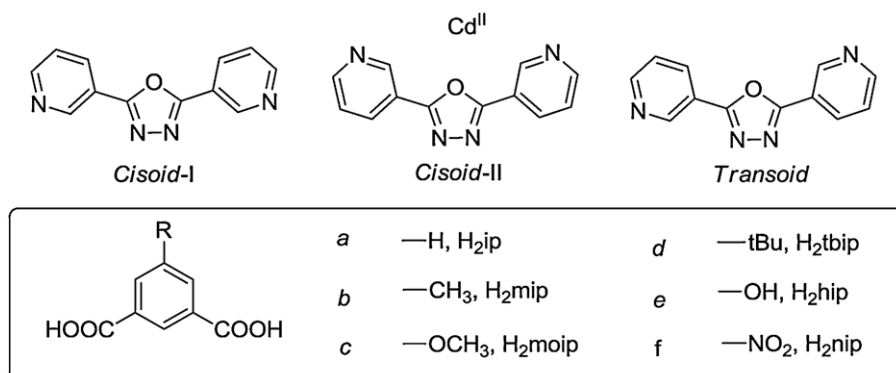


**Fig. 13.** (a) 1D molecular ladder array in  $\{[\text{Cd(ip)}(3,3'\text{-abpt})(\text{H}_2\text{O})](\text{H}_2\text{O})_{1.5}\}_n$  (**16a**). (b) 2D layered structure in  $\{[\text{Cd}_2(\text{nip})_2(3,3'\text{-abpt})_2(\text{H}_2\text{O})_4](\text{H}_2\text{O})_2\}_n$  (**16b**). (c) 1D chain motif in  $\{[\text{Cd(Htma)}(3,3'\text{-abpt})(\text{H}_2\text{O})_2](\text{H}_2\text{O})\}_n$  (**16c**) [102].

(see Fig. 14f). Other mixed-ligand CP systems containing the 3-bpo building block are also observed to be structurally modulated by the substituent effect of carboxyl-involved co-ligands [104,109].

The versatile ligand bpe, as a bifunctional building block [110,111], and the derivatives of the familiar dicarboxylate ligands isophthalate and terephthalate, with coordination-inert groups (such as  $-\text{SO}_3\text{H}$ ,  $-\text{NH}_2$ , and  $-\text{Br}$ ) are used to assemble

new CPs with Ag<sup>I</sup> (Scheme 19, see a–e) [112].  $[\text{Ag(ip)}_{0.5}(\text{bpe})]_n$  (**18a**) represents a 3D polymeric lattice that crystallizes in the acentric space group  $Fdd2$ , where both ip and bpe ligands play the bridging roles to extend the Ag<sup>I</sup> centers to afford a 3D ths network (see Fig. 15a). When H<sub>2</sub>ip is replaced by H<sub>3</sub>sip, a 2D layered CP  $\{[\text{Ag}_3(\text{sip})(\text{bpe})_2(\text{H}_2\text{O})](\text{H}_2\text{O})\}_n$  (**18b**) is obtained, where the sulfonate group of sip is involved in metal binding and the



**Scheme 18.** Illustration of the mixed-ligand assembled system with Cd<sup>2+</sup>, 3-bpo in different conformations, and a series of comparable R-isophthalic acids with different substituents, including (a) H<sub>2</sub>ip, (b) H<sub>2</sub>mip, (c) H<sub>2</sub>moip, (d) H<sub>2</sub>tbip, (e) H<sub>2</sub>hip, and (f) H<sub>2</sub>nip.

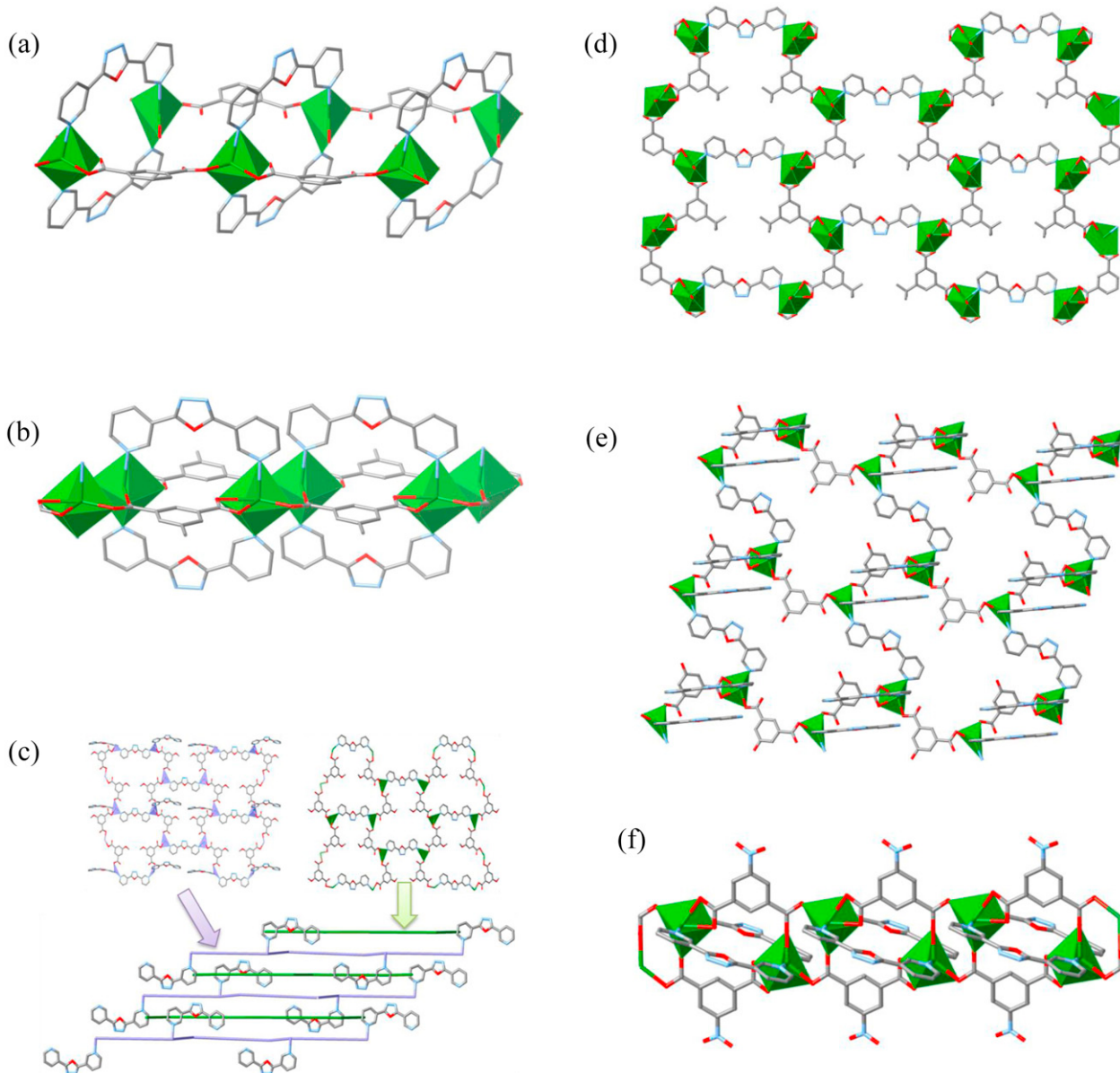
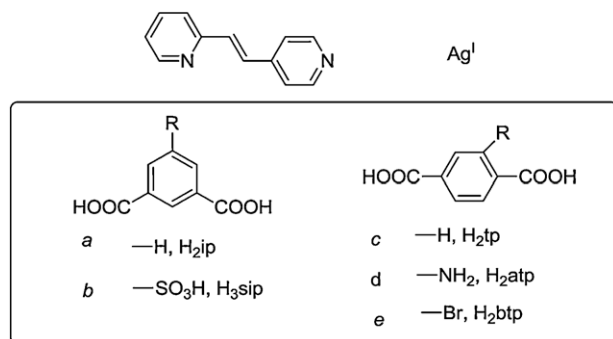


**Fig. 14.** Various Cd<sup>II</sup> networks assembled from 3-bpo and a series of *R*-isophthalic acids, including (a) H<sub>2</sub>ip, (b) H<sub>2</sub>mip, (c) H<sub>2</sub>moip, (d) H<sub>2</sub>tbip, (e) H<sub>2</sub>hip, and (f) H<sub>2</sub>nip [108].



**Scheme 19.** Illustration of the mixed-ligand assembled system with Ag<sup>I</sup>, bpe, and a series of comparable *R*-isophthalic acids or *R*-terephthalic acids with different substituents, including (a) H<sub>2</sub>ip, (b) H<sub>3</sub>sip, (c) H<sub>2</sub>tp, (d) H<sub>2</sub>atp, and (e) H<sub>2</sub>btp.

metal-ligand ratio is changed to 3:1. As a result, three different types of Ag<sup>I</sup> centers are connected by both sip and bpe ligands to form a new type of 2D (4.6<sup>2</sup>)(4<sup>3</sup>.6<sup>2</sup>.8)(4<sup>4</sup>.6<sup>6</sup>) topological net (see Fig. 15b). Further, the CPs  $[\text{Ag}(\text{tp})_{0.5}(\text{bpe})]_n$  (**18c**) and  $[\text{Ag}(\text{atp})_{0.5}(\text{bpe})]_n$  (**18d**) are isostructural with the 2D (6,3) layer (see Fig. 15c). Interestingly, the steric effect of —Br group in the btp tecton leads to the construction of a quite intricate 3D self-penetrating framework for  $\{[\text{Ag}_6(\text{btp})_2(\text{bpe})_4(\text{NO}_3)_2(\text{H}_2\text{O})](\text{H}_2\text{O})_2\}_n$  (**18e**) (see Fig. 15d), in which six types of Ag<sup>I</sup> centers with diverse coordination spheres and two btp<sup>2-</sup> ligands with  $\mu_3$ - and  $\mu_7$ -bridging modes are observed.

### 3. Other factors influencing the assembly of mixed-ligand CPs

Beyond the organic building blocks, the assembly of mixed-ligand CPs is sensitive to other factors such as solvent, pH, metal

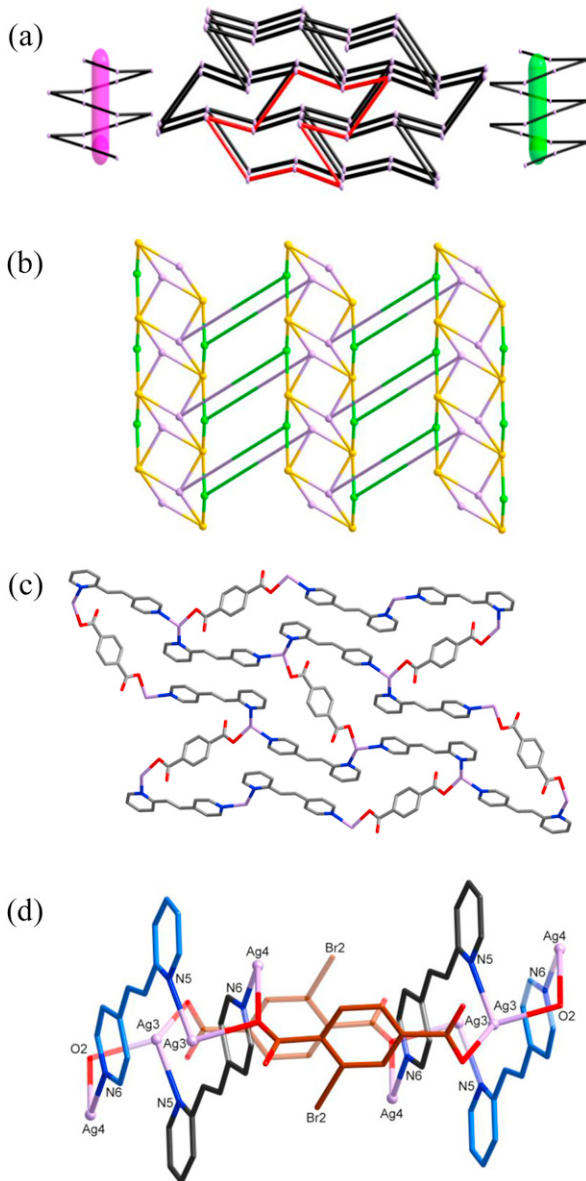


**Fig. 15.** Various Ag<sup>I</sup> coordination networks assembled from bpe and a series of benzene-dicarboxylic acids [112]. (a) H<sub>2</sub>ip, 3D framework of **ths** topology in **18a**. (b) H<sub>3</sub>sip, 2D network in **18b**. (c) H<sub>2</sub>tp and H<sub>2</sub>atp, 2D (6,3) layer in **18c** and **18d**. (d) H<sub>2</sub>btp, a portion of the self-penetrating pattern in **18e**.

ion, and synthetic route. Towards this objective, a number of typical examples will be discussed here, illustrating the fact that mixed-ligand CPs can be well modulated by such parameters to reveal their remarkable role in the construction of CPs.

### 3.1. Solvent

Generally, most CP systems are prepared from solvent media, but they are usually insoluble once synthesized, due to their polymeric nature. Thus, the choice of solvent is critical to achieve the phase-pure preparation of such crystalline materials and construct diverse coordination networks [113–116], taking account of reaction thermodynamics and activation energetics [117–119].

Two unusual solvent-controlled CPs have been obtained from the hydrothermal assemblies of NaH<sub>2</sub>sip and bpy with Cd<sup>II</sup> nitrate in EtOH-H<sub>2</sub>O and H<sub>2</sub>O solvents, respectively [120]. A 2D CP  $\{[Cd_2(sip)(bpy)_3(H_2O)_3][Cd(sip)(bpy)(H_2O)](H_2O)_8\}_n$  (**19a**) can be prepared in EtOH-H<sub>2</sub>O, consisting of cationic

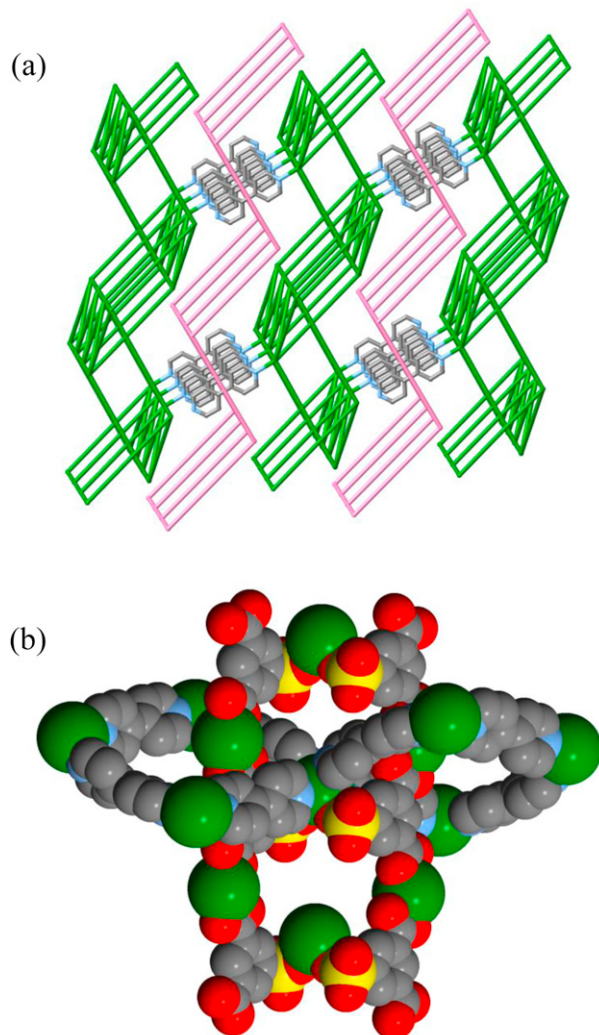


**Fig. 16.** Two different Cd<sup>II</sup> CPs involving mixed ligands sip and bpy, generated from different solvents. (a) EtOH-H<sub>2</sub>O, the interdigitating architecture of the cationic and anionic layers in **19a**. (b) H<sub>2</sub>O, the self-interpenetration pattern in **19b** [120].

$[Cd_2(sip)(bpy)_3(H_2O)_3]_{n+}$  and anionic  $[Cd(sip)(bpy)(H_2O)]_{n-}$  layers. In the anionic layer, the Cd<sup>II</sup> centers are interconnected by the sip and bpy linkers to form a 2D step-like network, whereas the cationic layer displays a decorated 2D step-like pattern with the unidentate bpy terminals protruding from both sides. The two types of counterion layers are arranged in an alternate fashion, where the uncoordinated bpy end from the cationic layers penetrates into the cavities of the anionic layers to form a tightly stacked neutral lattice, with the aid of electrostatic forces and H-bonding interactions (see Fig. 16a). A similar reaction in H<sub>2</sub>O affords a distinct 3D self-penetrating framework  $\{[Cd_3(sip)_2(bpy)_4(H_2O)_2](H_2O)_3\}_n$  (**19b**), where two types of 1D patterns consisting of  $[Cd_4(sip)_4]$  and  $[Cd_4(bpy)_4]$  subunits, respectively, are entangled by interlocking and interweaving (see Fig. 16b).

Of further significance, the solvent-induced breathing effect of the dynamic mixed-ligand CPs has also been demonstrated. That is, expanding and shrinking of the pores within the coordination networks is often concomitant with hydration and dehydration processes (see Fig. 17a). In this regard, the hydration or dehydration induced dynamic conversions of interpenetrating grid-like frameworks with both open and closed phases can be viewed as a simple glide motion without cleavage of any coordination bonding (see Fig. 17b). For example, CP  $\{[Zn(tp)(bpy)_{0.5}](DMF)(H_2O)_{0.5}\}_n$  (**20a**) of 2-fold interpenetrating 3D framework represents an open phase

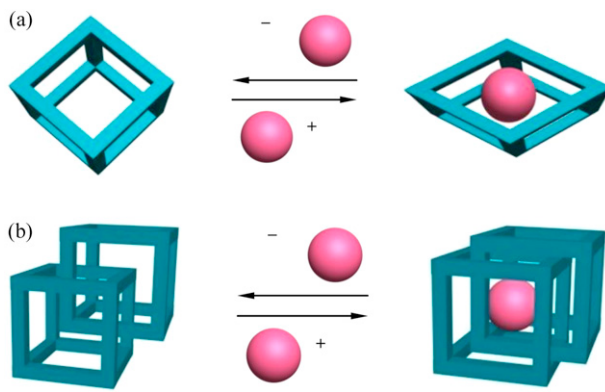


**Fig. 17.** Schematic representation of the solvent-induced breathing effect of dynamic coordination frameworks.

with the micropore size of  $4 \times 4 \text{ \AA}^2$ , in which the solvent molecules are included [121]. After dehydration, the resulting solvent-free phase  $[\text{Zn}(\text{tp})(\text{bpy})_{0.5}]_n$  (**20b**) will be non-porous with the unit-cell volume significantly decreased. Furthermore, this structural conversion is reversible by soaking **20b** in DMF-EtOH. Remarkably, the flexible nature of such a dynamic system will result in its application for separation of small molecules, such as *n*-pentane from *n*-hexane and 2-methylbutane from *n*-pentane, as well as hysteresis of gas sorption.

### 3.2. pH condition

In some cases, the pH of a coordination assembled system can also influence the crystalline product, probably in different ways such as adjusting the existing forms and binding fashions of carboxyl ligands, creating hydroxo bridges, and activating the assembling reactions, etc. [18].

For example, the pH of the reaction solution is critical to yield diverse products for the mixed-ligand CP system of  $\text{Cd}^{II}$ , 3-bpo, and  $\text{H}_3\text{sip}$  [21]. In this case, two completely different CPs  $\{[\text{Cd}_3(\text{sip})_2(3-\text{bpo})_2(\text{H}_2\text{O})_6](\text{H}_2\text{O})_{4.5}\}_n$  (**21a**) and  $\{[\text{Cd}(\text{sip})(3-\text{Hbpo})(\text{H}_2\text{O})](\text{H}_2\text{O})_2\}_n$  (**21b**) can be obtained at pH of ca. 2.5 and 4.0, respectively, which show the 2D layer and 1D tape polymeric motifs. Notably, the pH of reaction solutions will be decreased after crystallization ( $\Delta\text{pH} \approx 1$  for **21a** and 1.4 for **21b**). A possible explanation for this result is that the isolation of two such CPs incorporating the  $\text{sip}^{3-}$  component will increase the concentration of hydrogen ion in the mother liquor caused by the complete deprotonation of  $\text{H}_3\text{sip}$ . Of further importance, a similar pH effect is found in the mixed-ligand coordination system of  $\text{Cd}^{II}$ , 4-bpo, and  $\text{H}_3\text{sip}$ , but is not valid when other metal ions are present ( $\text{Co}^{II}$ ,  $\text{Ni}^{II}$ , and  $\text{Pb}^{II}$ ), indicating its specific selectivity to  $\text{Cd}^{II}$ .

In comparison, such pH effects impose more significant influences on coordination systems involving multicarboxylic acids as ligands, which can be rationally realized by gradually adjusting the deprotonation and binding modes of such tectons. For example, the assembly of  $\text{H}_4\text{bptc}$ , bpea, and  $\text{Cu}^{II}$  at pH values of 3, 4, and 7, respectively, can afford three different CPs [122]. The CP  $[\text{Cu}(\text{H}_2\text{bptc})(\text{bpea})(\mu_2-\text{H}_2\text{O})]_n$  (**22a**) is isolated at a lower pH value of 3, where the partly deprotonated  $\mu_2-\text{H}_2\text{bptc}$  ligands decorate the infinite metal–water chains that are pillared by the bpea ligands to form a 3D open framework (see Fig. 18a). When the pH is increased to 4,  $\{[\text{Cu}_3(\text{Hbptc})_2(\text{bpea})_3(\text{H}_2\text{O})_8](\text{H}_2\text{O})_4\}_n$  (**22b**) is formed, comprising two independent polymeric patterns in the same crystal, i.e. 1D  $[\text{Cu}(\text{bpea})(\text{H}_2\text{O})_4]_{n^{2+}}$  chain and 2D  $[\text{Cu}_2(\text{Hbptc})_2(\text{bpea})_2(\text{H}_2\text{O})_4]_{n^{2-}}$  layer, where the Hbptc ligands connect the  $\text{Cu}^{II}$  ions as tridentate linkers. The two types of motifs take an alternate stacking fashion in the lattices with a sequence of

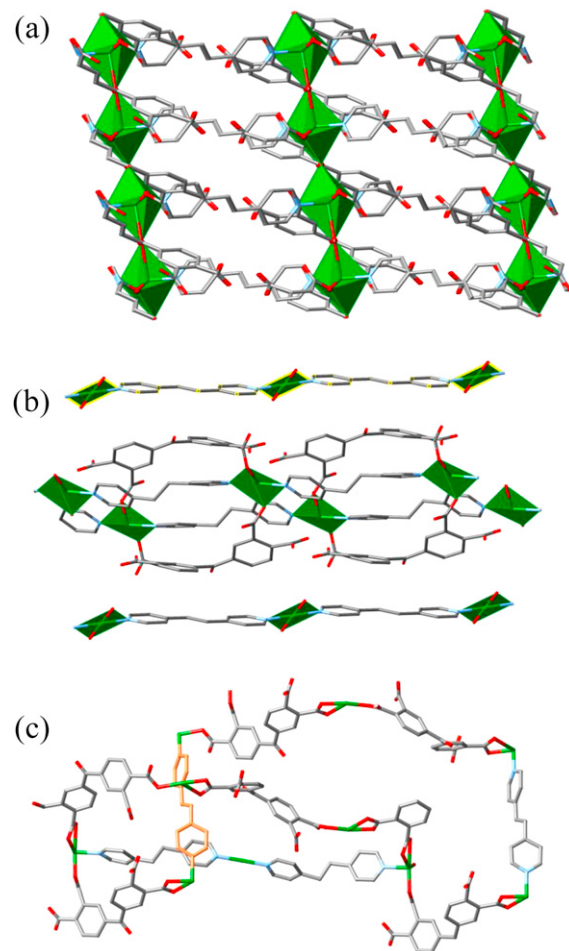


**Fig. 18.** Three different CPs isolated at different pH values by assembling  $\text{H}_4\text{bptc}$  and bpea with  $\text{Cu}^{II}$ . (a) pH 3, 3D open rhombic framework in **22a**. (b) pH 4, stacking pattern of the 1D cationic chains and 2D anionic layers in **22b**. (c) pH 7, self-interpenetrating unit of the 3D network in **22c** [122].

ABAB to construct a 3D sandwich-like architecture (see Fig. 18b). By further increasing the pH to 7,  $\{[\text{Cu}_2(\text{bptc})(\text{bpea})_2(\text{H}_2\text{O})](\text{H}_2\text{O})_{6.5}\}_n$  (**22c**) can be obtained. In contrast to **22a** and **22b**, the completely deprotonated bptc ligand in **22c** takes a 4-connected mode, with two carboxylates in bidentate chelating and the other two in unidentate binding. Thus, the  $\text{Cu}^{II}$  centers are extended by both bptc and bpea connectors to result in a quite complicated 3D self-interpenetrating network (see Fig. 18c).

### 3.3. Metal ion

As one of the most common factors influencing the assembly of CPs, in contrast to those well-designed and versatile organic tectons, metal ions can be viewed as a family of controllable building blocks [123]. That is, one particular metal element with a given valence normally defines its intrinsic coordination preference and geometry [124–126].

In this context, a series of mixed-ligand CPs have been prepared under diffusion condition, by assembling  $\text{Ni}^{II}$ ,  $\text{Zn}^{II}$ ,  $\text{Ag}^I$ ,  $\text{Cd}^{II}$ ,  $\text{Cu}^{II}$ , or  $\text{Pb}^{II}$  nitrate with  $\text{H}_2\text{tbtp}$  and 4-bpo [127]. These CPs display various 1D to 3D structural patterns with different coordination geometries of the metal ions, clearly indicating the metal-directed assembly. In the  $\text{Ni}^{II}$ ,  $\text{Zn}^{II}$ ,  $\text{Ag}^I$ , and  $\text{Cd}^{II}$  CPs, though the metal centers take different coordination numbers (6 and 7) and geometries (octahedral and pentagonal-bipyramidal), they are invariably bridged by the tbtp ligands to afford 1D polymeric chains, with the uniden-

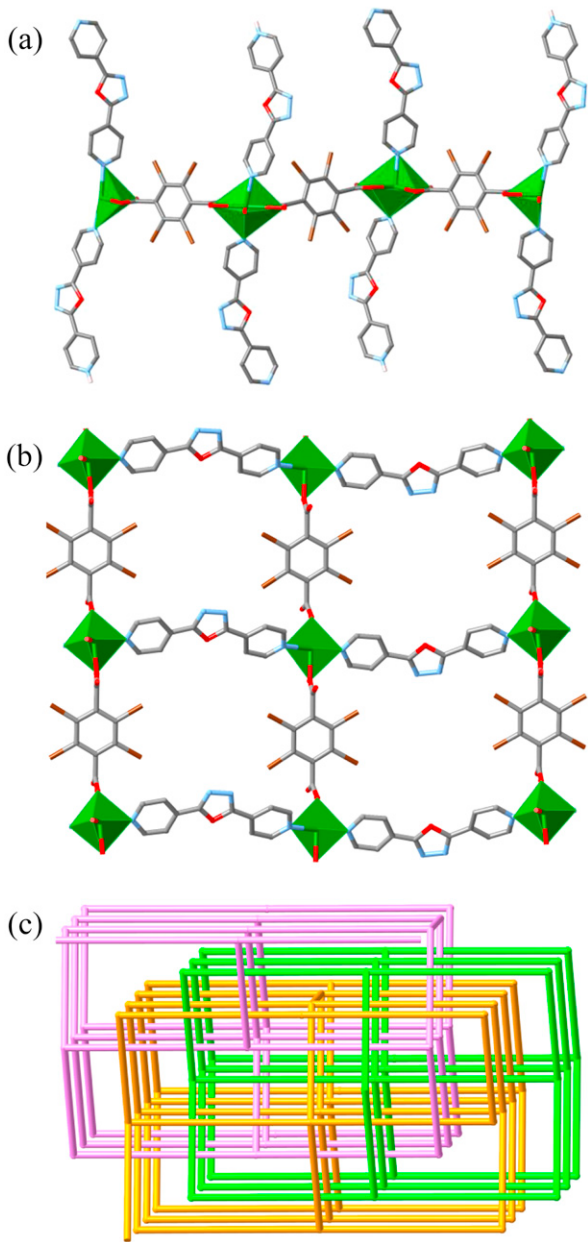


**Fig. 19.** Mixed-ligand CPs assembled from different metal ions with H<sub>2</sub>tbtp and 4-bpo. (a) Ni<sup>II</sup>, Zn<sup>II</sup>, Ag<sup>I</sup>, and Cd<sup>II</sup>, 1D polymeric chain motif. (b) Cu<sup>II</sup>, 2D (4,4) layered network. (c) Pb<sup>II</sup>, 3D 3-fold interpenetrating framework [127].

tate 4-bpo tectons decorating as pendant arms (see Fig. 19a). For the Cu<sup>II</sup> CP, the Cu<sup>II</sup> center adopts a distorted square-pyramidal sphere, and both the 4-bpo and tbtp ligands connect the Cu<sup>II</sup> ions as bidentate bridges to form a (4,4) coordination layer (see Fig. 19b). When the post-transition Pb<sup>II</sup> ion with an identifiable void for ligand disposition (namely, inert-pair effect) is employed, a distinct 3D CP is constructed. In this structure, the Pb<sup>II</sup> centers show distorted tetrahedral coordination spheres, which are connected by 4-bpo and tbtp ligands to afford a 3D **dia** open framework with 1D channels of ca. 14.1 × 11.6 Å<sup>2</sup>. Thus, each network is filled via catenation with two other networks to construct a 3-fold interpenetrating architecture (see Fig. 19c). In another case, reactions of 4,4'-abpt and H<sub>3</sub>tma with different metal salts (Co<sup>II</sup>, Ni<sup>II</sup>, and Cd<sup>II</sup>) yield a series of new CPs under hydrothermal conditions [128]. In the Co<sup>II</sup> and Ni<sup>II</sup> CPs, due to the similar octahedral coordination of metal centers, the resulting networks are isostructural and

exhibit 2D corrugated layers. With regard to the Cd<sup>II</sup> CP, the distorted pentagonal-bipyramidal Cd<sup>II</sup> centers are extended via the Htma bridges to produce a 1D linear array with 4,4'-abpt decorating on one side as the terminal ligands.

### 3.4. Synthetic route

Interestingly, different crystalline products of CPs can be obtained from the same reactants using distinct synthetic routes such as room-temperature solvent evaporation, layered-diffusion, and hydrothermal synthesis, etc. In this regard, some representative examples on the controlled preparation of CPs through different synthetic pathways have been illustrated [129]. For mixed-ligand CPs, hydrothermal reactions of Zn<sup>II</sup> with bpy and H<sub>2</sub>nip at 140 °C and 180 °C produce a 1D ribbon chain and a 2D layer, respectively [130,131]. Under the layered-diffusion route, another CP can be obtained, showing a 2D double layered structure [132]. Assemblies of Zn<sup>II</sup> nitrate with mixed ligands 4-bpo and H<sub>2</sub>tbtp using layered-diffusion or directly mixing route with solvent evaporation afford two distinct CPs with 1D chain and 2D layer patterns [127]. Assembly of Cd<sup>II</sup> with 4,4'-abpt and H<sub>3</sub>tma, using two synthetic routes such as solvent evaporation at room temperature and the hydrothermal reaction, yields a pair of different CPs with 2D layers and 1D chain structures, respectively [128].

## 4. Construction of specific CPs with mixed ligands

### 4.1. Unusual topological networks

Network topology is an important and essential aspect for the analysis and design of CPs and also of inherent significance for understanding the assembling laws therein. Towards this direction, complicated crystalline lattices can be appropriately simplified to equivalent node-and-rod nets, and new insights into engineering strategy of CPs are possible on the basis of topological consideration [6]. In mixed-ligand CP systems, new or unusual network topologies are of special focus, in virtue of the diverse connectivity of mixed ligands in structural construction.

Assemblies of the flexible ligand bpp and Co<sup>II</sup> with the isophthalate derivatives H<sub>2</sub>mip and H<sub>2</sub>tbip lead to two unique 4- and 6-connected 2D networks [133]. In [Co<sub>2</sub>(mip)<sub>2</sub>(bpp)<sub>2</sub>(H<sub>2</sub>O)]<sub>n</sub> (**23a**), both [Co<sub>2</sub>(COO)<sub>4</sub>] dimers and discrete Co<sup>II</sup> centers can be regarded as 4-connecting nodes, which are interconnected by mip and bpp bridges to afford an unusual 2D network (see Fig. 20a) with the Schläfli symbol (4.6<sup>4</sup>.8)<sub>2</sub>(4<sup>2</sup>.6<sup>4</sup>). Whereas in [Co<sub>2</sub>(tbip)<sub>2</sub>(H<sub>2</sub>tbip)(bpp)(H<sub>2</sub>O)]<sub>n</sub> (**23b**), two types of similar but independent [Co<sub>2</sub>(μ-COO)<sub>2</sub>(μ-H<sub>2</sub>O)] SBUs are connected by the dicarboxyl and bpp linkers to give a uninodal 6-connected 2D bilayer network with the Schläfli symbol (3<sup>3</sup>.4<sup>10</sup>.5.6) (see Fig. 20b).

To complicate the connectivity of organic tectons and further the resulting CP networks, aromatic multicarboxylic acids with suitable spacers can be used. For example, hydrothermal reactions of Mn<sup>II</sup> acetate with H<sub>3</sub>nbtc and different bipyridine ligands (bpy, bpea, and bpp) yield a series of 2D and 3D CPs [90]. In {[Mn<sub>3</sub>(nbtc)<sub>2</sub>(bpy)<sub>3</sub>(H<sub>2</sub>O)<sub>2</sub>](H<sub>2</sub>O)<sub>2</sub>}<sub>n</sub> (**24a**), the nbtc ligands can be simplified as 4-connected nodes, which interlink the 4- and 5-connected Mn<sup>II</sup> nodes with the aid of bpy bridges to construct a 3D (4,5)-connected network, with the Schläfli symbol (4<sup>2</sup>.6<sup>7</sup>.8)(6<sup>4</sup>.8<sup>2</sup>)(4<sup>2</sup>.6<sup>4</sup>). When the rigid bpy rod is replaced by the flexible bpea tecton, a 2D CP {[Mn<sub>3</sub>(nbtc)<sub>2</sub>(bpea)(H<sub>2</sub>O)<sub>5</sub>](bpea)<sub>0.5</sub>(H<sub>2</sub>O)}<sub>n</sub> (**24b**) is obtained, where the μ<sub>4</sub>- and μ<sub>5</sub>-nbtc anions serve as the 4- and 5-connected nodes to afford a very complicated (3,4,5)-connected network with two types of 3-connected Mn<sup>II</sup> ions. In another CP [Mn<sub>3</sub>(nbtc)<sub>2</sub>(bpp)<sub>2</sub>(H<sub>2</sub>O)<sub>4</sub>]<sub>n</sub> (**24c**), each nbtc anion is linked to four metal centers and can be regarded as a 4-connected node. In com-

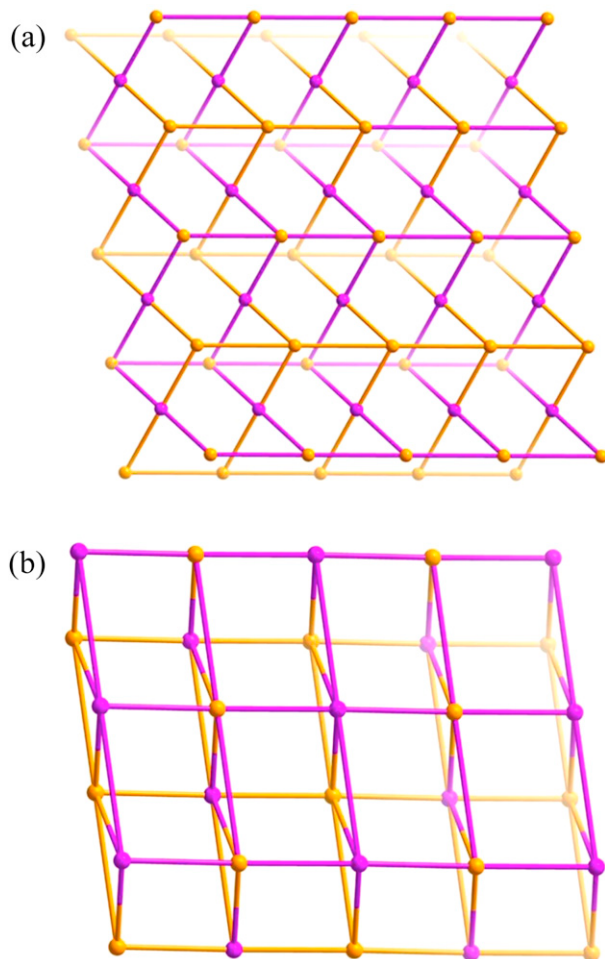


**Fig. 20.** Schematic representation of (a) 4-connected 2D network topology in **23a**, and (b) 6-connected 2D bilayer topology in **23b** [133].

bination with the 3-connected Mn<sup>II</sup> ions, a layered (3,4)-connected network with (4<sup>2</sup>.6)(4<sup>2</sup>.6<sup>3</sup>.8) topology is constructed, with the unidentate bpp ligands decorating at two sides.

#### 4.2. Entangled networks

Entanglement represents one of the most typical structural styles of supramolecular architectures. Compared with the familiar interpenetrating patterns, the self-penetrating networks that can be considered as the polymeric equivalent of molecular knots, are much less known at present [105,134–137]. Of particular interest, such intriguing networks are readily constructed by using the mixed-ligand strategy, due to both flexibility and multi-connectivity of different ligands involved within the same framework [138–140].

The fluorinated H<sub>2</sub>tfpbpp ligand has been applied to construct Zn<sup>II</sup> coordination networks with isophthalate co-tecrons [106], as a promising flexible bidentate building block to design entangled patterns. Reactions of H<sub>2</sub>tfpbpp and Zn<sup>II</sup> with H<sub>2</sub>ip or H<sub>2</sub>mip produce two isostructural CPs, showing the unprecedented 2-fold interpenetrating architecture of 3D self-penetrating nets. In detail, the H<sub>2</sub>tfpbpp pillars are inclined to interlink the 2D [Zn(ip)]<sub>n</sub> or [Zn(mip)]<sub>n</sub> layers into a rare **mab** framework of (4<sup>4</sup>.6<sup>10</sup>.8) topology with self-penetrating feature. Remarkably, each self-penetrating **mab** net possesses large voids to facilitate the formation of a 2-fold interpenetrating lattice (see Fig. 21a). However, when similar dicarboxyl tectons H<sub>2</sub>fip or H<sub>2</sub>nip are used instead, the resulting

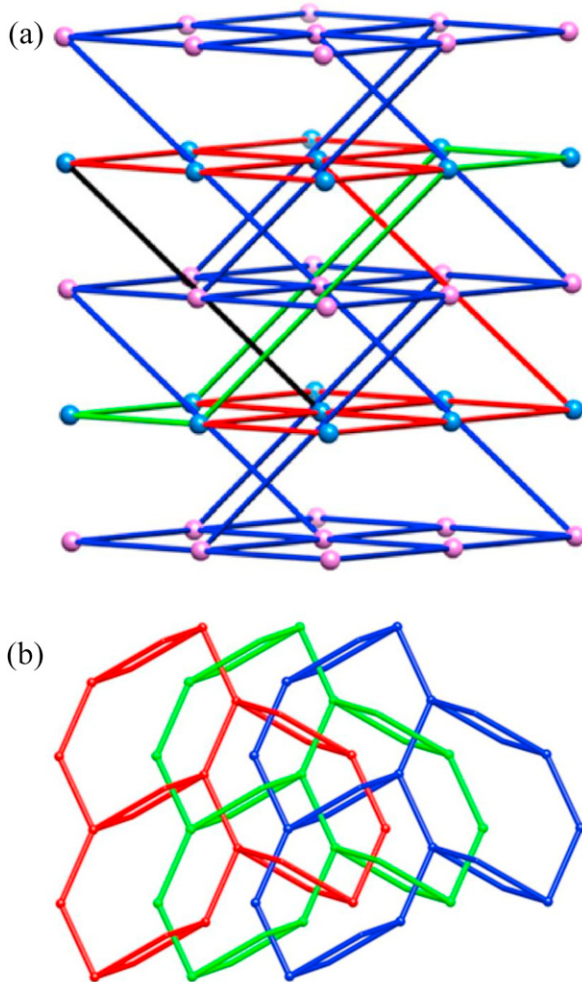


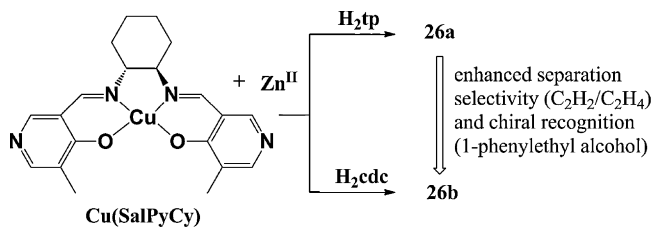
**Fig. 21.** Schematic representation of (a) two interpenetrating **mab** networks, each of which is also a self-interpenetrating pattern, and (b) 3-fold parallel interpenetration of **hcb** layers with polyrotaxane character [106].

CPs have distinct 2D **hcb** networks with both 3-fold interpenetration and polyrotaxane characteristics. Each hexagonal subunit of the **hcb** layer consists of four fip or nip bridges and two doubly bridged H<sub>2</sub>tfpbpp loops, which provide the suitable spaces for holding the rods from other two layers and thus result in a parallel interpenetration with the features of a polyrotaxane (see Fig. 21b).

#### 4.3. Chiral networks

Stable chiral CPs are currently of special interest owing to their promising applications in enantioselective sorption, separation, and catalysis. Generally, there are two eligible approaches to achieve such chiral crystalline materials, namely using a chiral tecton as the primary linker or auxiliary co-ligand, and using the achiral building blocks via spontaneous resolution [141].

Construction of chiral coordination assemblies with achiral ligands can also be realized by chiral induction, that is, to induce chirality of the crystal products via the external stimulator, usually chemical in nature [141]. In general, such a strategy may be accomplished using chiral solvents (organic solvent and ionic liquid) [142,143] or chiral additive agents [144,145], which may provide particularly weak interactions, such as solvent–solute contacts, van der Waals forces, hydrogen bonds, and π···π stacking, etc. However, the origin of most supramolecular chirality in CPs is so far ambiguous. For instance, using the achiral mixed



**Scheme 20.** Illustration of the synthetic route and separation capacity of enantiopure mixed-ligand CPs **26a** and **26b**, constructed by chiral Cu-salen metalloligand, Zn<sup>II</sup>, and different dicarboxylic acids (H<sub>2</sub>tp or H<sub>2</sub>cdc).

ligands H<sub>3</sub>btc and tib and controlling the pH of the reaction generates a pair of unique 3d-3d heterometallic CPs [146]. {[Zn<sub>2</sub>Co(tib)<sub>3</sub>(H<sub>2</sub>O)<sub>5</sub>][Zn<sub>6</sub>(tib)<sub>2</sub>(btc)<sub>6</sub>](H<sub>2</sub>O)<sub>12.7</sub>}<sub>n</sub> (**25a**) isolated at pH 8–9 crystallizes in the hexagonal space group *P*6<sub>3</sub> and consists of two separated 2D fragments, which are arranged in an ABCD stacking fashion with the cationic and anionic layers in an alternating location. However, {[ZnCo(tib)(btc)(H<sub>2</sub>O)<sub>2</sub>]Cl(H<sub>2</sub>O)<sub>3</sub>}<sub>n</sub> (**25b**) prepared at pH 5–6 crystallizes in space group *P*2<sub>1</sub>2<sub>1</sub>2<sub>1</sub> and features a chiral binodal 3-connected framework of (12<sup>2</sup>.14)(12<sup>3</sup>) topology, where the 1D helical chains and the 1D achiral chains are arranged alternately. Elsewhere, the use of 1-butyl-3-methyl imidazolium *L*-asp as solvent and/or template to synthesize chiral compounds undoubtedly reveals its chiral induction effect [142].

Conceptually, the easiest way to achieve a chiral crystalline solid is to use a chiral component as a starting point. Especially in mixed-ligand CP systems, the combination of pyridine derived ligand and amino acid represents an effective method to obtain the targeted chiral crystals. For example, the solvothermal reaction of Ni<sup>II</sup>, *L*-asp, and bpy produces a chiral open framework material [147], in which the chiral [Ni(*L*-asp)]<sub>n</sub> layers are extended by the achiral bpy linkers to form a pillared 3D structure with 1D channels for guest accommodation. Interestingly, careful control over the water/methanol ratio results in an achiral structure, caused by the racemization of starting amino acid at a higher concentration of water. In another case, three isoreticular homochiral porous CPs can be readily prepared from Zn<sup>II</sup>, (+)-H<sub>2</sub>cam, and rigid linear N-donor spacers, such as dabco, bpy, and bpee [148]. The lengths of these linear ligands will modulate the pore sizes and free accessible volumes of the homochiral CPs. Other chiral mixed-ligand CPs with H<sub>2</sub>cam have also been reported [149,150].

Recently, Chen and co-workers have developed a metalloligand or pre-constructed building block approach to construct the enantiopure mixed-ligand CPs, that is, using chiral M-salen metalloligands and M'-dicarboxylates units to obtain the targeted chiral materials (see Scheme 20) [151]. The hydrothermal reactions of the chiral metalloligand Cu(SalPyCy) with Zn(NO<sub>3</sub>)<sub>2</sub> and H<sub>2</sub>tp or H<sub>2</sub>cdc can readily form the chiral CPs {[Zn<sub>3</sub>(tp)<sub>3</sub>][Cu(SalPyCy)][(DMF)<sub>5</sub>(H<sub>2</sub>O)<sub>4</sub>]}<sub>n</sub> (**26a**) or {[Zn<sub>3</sub>(cdc)<sub>3</sub>][Cu(SalPyCy)][(DMF)<sub>5</sub>(H<sub>2</sub>O)<sub>4</sub>]}<sub>n</sub> (**26b**). In both structures, the [Zn<sub>3</sub>(COO)<sub>6</sub>] SBUs are connected by tp or cdc anions to afford the 3<sup>6</sup> tessellated [Zn<sub>3</sub>(tp)<sub>3</sub>]<sub>n</sub> or [Zn<sub>3</sub>(cdc)<sub>3</sub>]<sub>n</sub> sheets, which are further pillared by Cu(SalPyCy) building blocks to construct the isostructural chiral 3D frameworks involving two chiral pore cavities with a diameter of ca. 6.4 Å. Significantly, the desolvated solids **26a** and **26b** show a highly selective separation of C<sub>2</sub>H<sub>2</sub> and C<sub>2</sub>H<sub>4</sub> (1.6 vs 25.5) and the enantioselective separation of *S*-1-phenylethyl alcohol (ee = 21% vs 64%), indicating their potential applications in practical adsorption-based separation.

## 5. Physicochemical properties and applications

Many well-designed CPs with mixed-ligand tectons show fascinating physicochemical properties, such as adsorption, separation, magnetism, optics, conductivity, and catalysis, etc. [152–157].

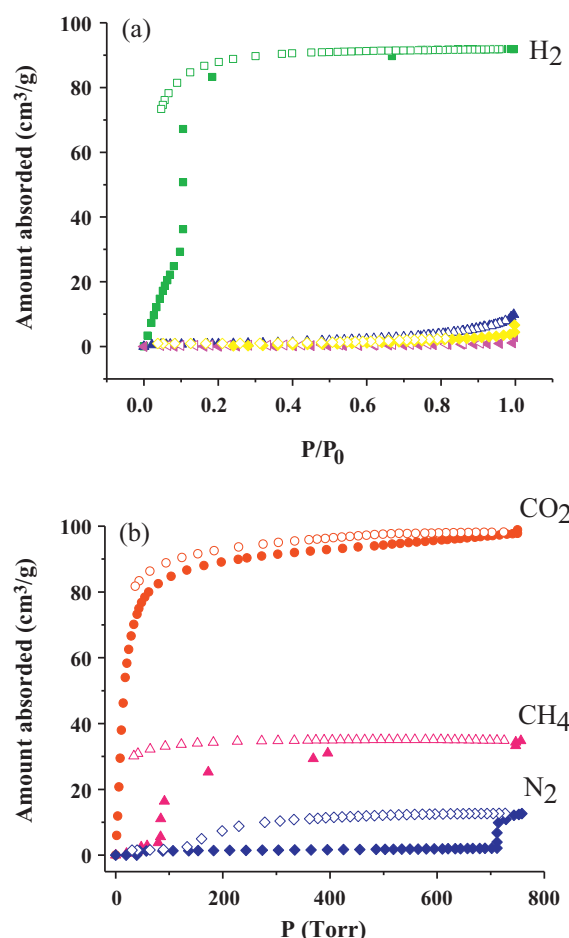


**Fig. 22.** Gas sorption isotherms of **27c** at (a) 77 K (H<sub>2</sub>, green; N<sub>2</sub>, blue; Ar, magenta; CO, yellow) and (b) 195 K (CO<sub>2</sub>, red; CH<sub>4</sub>, pink; N<sub>2</sub>, blue). Reprinted from Ref. [158]. Copyright 2007, with permission from American Chemical Society.

Notably, herein we mainly focus on the representative CPs which show the obvious changes of material properties concomitant with the delicate modification of the mixed-ligand building components, in order to explore further the potential structure–property correlation of CPs based on the mixed-ligand synthetic strategy.

### 5.1. Gas adsorption and separation

The delicate control and tuning of small pore or window sizes for the open frameworks of CPs is crucial to achieve highly effective storage and separation of guest molecules by the size-exclusion effect, in which the small substrates can go through the pore channels. In this regard, a simple strategy to construct the desired channels or cavities of coordination networks by regulating the types of mixed-ligand components is of particular interest and significance.

Hydrothermal reactions of Cu<sup>II</sup> nitrate with H<sub>2</sub>fma and three comparable bipyridine linkers (pyz, bpy, and bpee) result in similar 3D primitive cubic frameworks [Cu(fma)(pyz)<sub>0.5</sub>]<sub>n</sub> (**27a**), {[Cu(fma)(bpy)<sub>0.5</sub>](H<sub>2</sub>O)<sub>0.25</sub>]<sub>n</sub> (**27b**), and {[Cu(fma)(bpee)<sub>0.5</sub>](H<sub>2</sub>O)<sub>0.5</sub>]<sub>n</sub> (**27c**), which are doubly interpenetrating [158]. The void spaces in these CPs can be systematically tuned, simply by modifying the bipyridine pillars. Of further interest, CP **27c** shows selective gas adsorption behavior. In fact, the 2.0 × 3.2 Å<sup>2</sup> pores in **27c** are larger than the size of H<sub>2</sub> (2.8 Å) but smaller than those of N<sub>2</sub> (3.64 Å) and CO (3.64 Å). Thus, it exhibits significant selectivity of H<sub>2</sub> uptake over CO and N<sub>2</sub> at 77 K (see Fig. 22a) and also, selective sorption of CO<sub>2</sub> (3.3 Å)

over CH<sub>4</sub> (3.8 Å) at 195 K (see Fig. 22b). Notably, owing to the structural flexibility, such a microporous material also shows different hysteresis sorption behaviors with respect to H<sub>2</sub>, N<sub>2</sub>, CO<sub>2</sub>, and CH<sub>4</sub>.

A series of mixed-ligand CPs are built from the robust [Zn<sub>2</sub>(COO)<sub>4</sub>] paddle-wheel subunits and three different dicarboxylate linkers (H<sub>2</sub>fma, H<sub>2</sub>tp, and 2,6-H<sub>2</sub>ndc) to define the perforated 2D layers, which are further pillared by the bpy rods to form 3D open coordination frameworks with the inclusion of solvents [159]. For the desolvated samples, only tp-involved CP exhibits significant N<sub>2</sub> adsorption behavior with an approximate type I Langmuir isotherm and the BET surface area of 660 m<sup>2</sup>/g. Similar examples of the mixed-ligand microporous CPs with adjustable gas adsorption have also been reported [160–162].

Of further interest, some flexible mixed-ligand CPs possess voids that are too small to allow guest entrance, which however may exhibit a gate-opening character to expand for gas adsorption. In this regard, the 2D CP {[Cu<sub>2</sub>(dhbc)<sub>2</sub>(bpy)](H<sub>2</sub>O)}<sub>n</sub> with 2-fold interdigitated pattern undergoes a drastic crystal transformation triggered by desorption of water guest to result in a cell-volume contraction [163]. Actually, such a structural change is accompanied by a shrinking of the layer gap arising from the glide motion of two dhbc moieties, which leads to a decrease of the channel cross-section. When exposing the dehydrated solid to N<sub>2</sub> vapor at the gate-opening pressure, structural re-expansion is reversibly observed. Notably, this CP shows characteristic hysteresis adsorption isotherms, with different gate-opening and gate-closing pressures for CO<sub>2</sub> and other super critical gases (CH<sub>4</sub>, O<sub>2</sub>, and N<sub>2</sub>).

Similar gate-open adsorption phenomena are also observed in {[Cu<sub>2</sub>(pzdc)<sub>2</sub>(bpg)]<sub>n</sub>} which is constructed by the bridging pzdc ligands and flexible bpg linkers. Significantly, with regard to the gate-opening process herein, H-bonding is the critical driving force. In this case, the 2D {[Cu<sub>2</sub>(pzdc)<sub>2</sub>]<sub>n</sub>} layers are pillared by the bpg ligands to form a 3D network with 1D narrow channels, in which the hydroxyl groups of bpg are exposed to form H-bonding with the guests [164]. From the adsorption isotherms of MeOH and H<sub>2</sub>O vapors as well as CH<sub>4</sub> at 298 K, a specific adsorption of MeOH or H<sub>2</sub>O will occur under the proper pressure, whereas CH<sub>4</sub> cannot be adsorbed. Moreover, the desorption isotherm does not trace the adsorption isotherm, which indicates a dynamic structural transformation of the framework. Therefore, this selective adsorption can be primarily associated with the H-bonding interactions between MeOH or H<sub>2</sub>O molecules and hydroxyl groups of the bpg ligands.

## 5.2. Magnetism

Due to the complexity and difficulty in controlling the organic magnetic carriers [154], the rational design and construction of mixed-ligand magnetic CPs still remains a great challenge, in contrast to that of pure inorganic and other organic–inorganic hybrid materials with simpler magnetic bridges. However, this strategy will also result in diverse CP magnetic behaviors, which, in some cases, may be well regulated by proper modification of the ligand components.

Assemblies of Cu<sup>II</sup> and H<sub>2</sub>mma with pyz or bpy produce two 3D CPs, {[Cu<sub>2</sub>(mma)<sub>2</sub>(pyz)]<sub>n</sub>} (**28a**) and {[Cu<sub>2</sub>(mma)<sub>2</sub>(bpy)(H<sub>2</sub>O)<sub>2</sub>]<sub>n</sub>} (**28b**), respectively [165]. The structures of both CPs are similar, composed of corrugated layers of Cu<sup>II</sup> (**28a**) and water–Cu<sup>II</sup> (**28b**) units with intralayer methylmalonate bridges in *anti-syn* (equatorial–apical) coordination mode and additional pyz or bpy pillars. Magnetic susceptibility measurements of **28a** and **28b** in the temperature range of 2–300 K reveal the occurrence of two types of magnetic interactions: ferromagnetic coupling through the

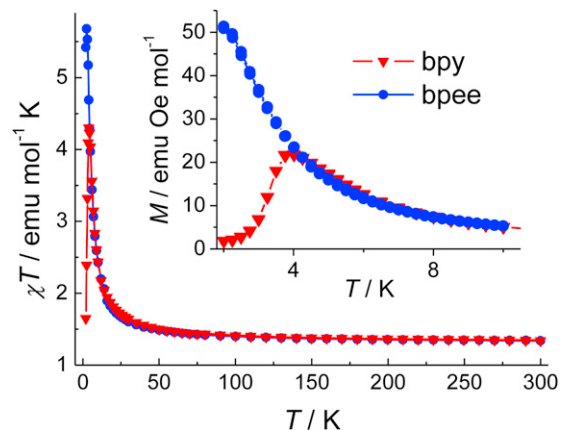


**Fig. 23.**  $\chi T$ - $T$  plots at 2 kOe for the two Ni<sup>II</sup> CPs with H<sub>2</sub>ndc and bpy or bpee auxiliary ligand. The inset shows the coincident ZFC and FC magnetizations for each CP at 20 Oe.

Reprinted from Ref. [167]. Copyright 2010, with permission from the Royal Society of Chemistry.

carboxylate bridges (**28a** and **28b**) and antiferromagnetic exchange through pyz (**28a**) or bpy (**28b**) linkers. However, the corrugated malonate-bridged Cu<sup>II</sup> layers in {[Cu<sub>4</sub>(mal)<sub>4</sub>(bpee)<sub>3</sub>](H<sub>2</sub>O)<sub>6</sub>}<sub>n</sub> (**28c**) are extended by the bis-unidentate bpee ligands to afford a 3D coordination network [166]. The Cu<sup>II</sup> ions in the layers are bridged by a double  $\mu$ -oxo and four carboxylato-malonate linkers, which will induce an overall ferromagnetic behavior.

Two 3D mixed-ligand Ni<sup>II</sup> CPs can be obtained from H<sub>2</sub>ndc and the comparable bipyridine ligands (bpy and bpee), where the mother framework [Ni(nndc)]<sub>n</sub> is flexible enough to be pillared by different auxiliary co-ligands [167]. Remarkably, the variation of ligands from bpy to bpee will not influence the network topology but result in a significant magnetic transformation from metamagnetism to paramagnetism (see Fig. 23). This illustrates a nice example for controlling the magnetic behavior of mixed-ligand CPs. In another case, a family of Mn<sup>II</sup> CPs are prepared from the mixed ligands bpy and three comparable aliphatic acids (H<sub>2</sub>suc, H<sub>2</sub>glu, and H<sub>2</sub>adi), showing a 3D open framework (**29a**), 2D layer (**29b**), and 2-fold interpenetrating 3D architecture (**29c**), respectively [168]. Interestingly, the antiferromagnetic interactions between Mn<sup>II</sup> ions in **29a**–**29c** will be stronger when the spacer lengths of aliphatic acids are increased.

## 5.3. Catalysis

Although CPs still cannot completely replace inorganic materials, such as the classical molecular sieves and zeolites in catalysis, CPs can be considered as the good candidates for fine organic synthesis and enantioselective catalysis under mild conditions [169]. Generally, the CP catalytic activity may originate from the open metal sites, reactive functional groups, and host matrices or nanometric reaction cavities [170]. For example, three 3D CPs with Co<sup>II</sup>, Ni<sup>II</sup>, and Zn<sup>II</sup> as active metal sites can be prepared based on the mixed ligands H<sub>2</sub>oba and bpy [82]. The various metal polyhedra of Co<sub>4</sub>N trigonal-bipyramidal, NiO<sub>4</sub>N<sub>2</sub> octahedron, and ZnO<sub>4</sub> tetrahedron or ZnO<sub>3</sub>N<sub>2</sub> trigonal-bipyramidal facilitate their different photocatalytic activities for degradation of some organic dyes, such as orange G, rhodamine B, Remazol Brilliant Blue R, and methylene blue (see Fig. 24). Further, by introducing U<sub>5</sub>O<sub>14</sub> units into the Ni<sup>II</sup> mixed-ligand CP with H<sub>2</sub>pydc and bpy, a 3D microporous hybrid material showing photocatalytic activity for degradation of methyl blue as a model pollutant [171], can be obtained under hydrothermal conditions.

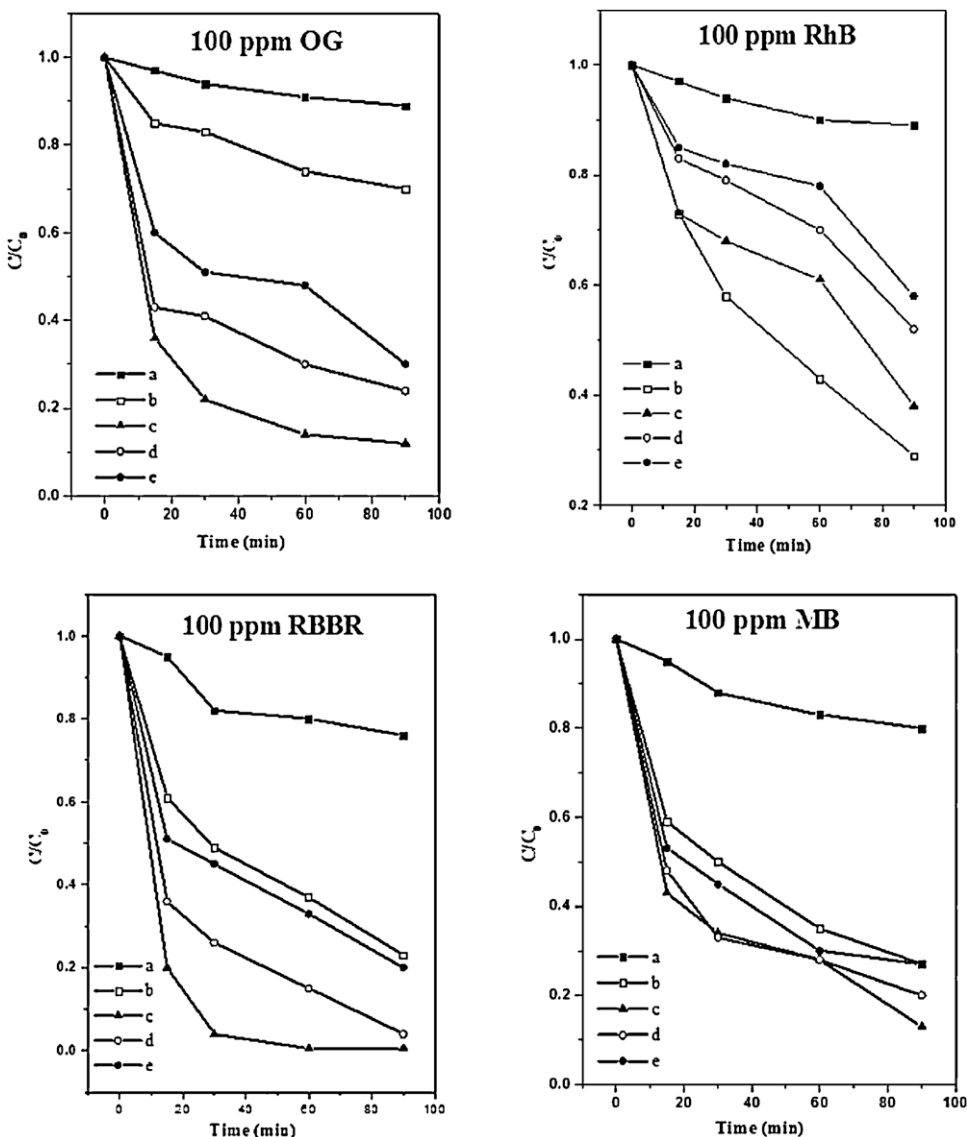


**Fig. 24.** Degradation profiles of four dyes with an initial concentration of 100 ppm: (a) without catalyst, (b) with Degussa P-25, (c) with Co<sup>II</sup> CP, (d) with Ni<sup>II</sup> CP, and (e) with Zn<sup>II</sup> CP.

Reprinted from Ref. [82]. Copyright 2006, with permission from American Chemical Society.

The pillared-layer CPs  $[\text{Cu}_2(\text{pzdc})_2(\text{L})]_n$  ( $\text{L} = \text{pyz}$ , **30a**; bpy, **30b**; bpee, **30c**) have similar 1D channels of different sizes of  $4.0 \times 6.0$ ,  $8.2 \times 6.0$ , and  $10.3 \times 6.0 \text{ \AA}^2$ , respectively, within which the carboxylate oxygen atoms of pzdc display Lewis basic nature to serve as specific adsorption sites for alkynes, leading to the realization of anionic polymerization [172,173]. For instance, methyl propionate will polymerize inside the channels of **30b** upon standing at room temperature, and the structure of CP is preserved before and after polymerization. Further, the poly(methyl propionate) can be recovered from the CP by extracting the solid with DMF at 353 K. The polymer displays mostly a *trans*-configuration of the C=C double bonds. Of further importance, such a polymerization reaction suffers a spatial confinement effect. That is, the reaction cavities provided by these CPs with a precise arrangement of carboxylate oxygen donors and the proper adsorption sites for different acetylene monomers (acetylene or methyl propionate) is responsible for the successful polymerization, by enabling the strong interaction between the monomer and carboxylate.

## 6. Conclusion

The aim of this review is to present a brief summary to examine the broad relationship between the nature of each type of ligand component in the mixed-ligand CP systems and the structures and properties of the resulting polymeric architectures, in order to portray a guideline for the design of organic tectons and further the targeted crystalline solids. In this direction, the most effective approach for structural construction of mixed-ligand CPs is to combine both acid and base ligands within the same assembled system, rather than the acid–acid or base–base system. Further, the design of organic tectons is mostly practiced by modifying the ligand backbones containing carboxyl, pyridine, diazolyl, and triazolyl functional groups. Moreover, the mixed-ligand synthetic strategy will be highly affected by the spacer effect, positional isomeric effect, and substituent effect of either type of organic ligands, as well as some other factors including solvent, pH, metal ion, and synthetic route. These can establish an essential methodology for

the rational design and construction of the desired CPs with promising properties and potential applications.

## Acknowledgments

We thank the National Natural Science Foundation of China (Nos. 20971098, 21031002, and 21171151), Tianjin Natural Science Foundation (No. 10JCZDJC21800), Plan for Scientific Innovation Talent of Henan Province, Program for New Century Excellent Talents in University, and Tianjin Normal University for financial support.

## References

- [1] G.R. Desiraju, *Angew. Chem. Int. Ed.* 46 (2007) 8342.
- [2] D. Braga, F. Greponi, *Chem. Commun.* (2005) 3635.
- [3] S.R. Batten, N.R. Champness, X.M. Chen, J. Garcia-Martinez, S. Kitagawa, L. Öhrström, M. O'Keeffe, M.P. Suh, J. Reedijk, *CrystEngComm* 14 (2012) 3001.
- [4] J.P. Zhang, X.C. Huang, X.M. Chen, *Chem. Soc. Rev.* 38 (2009) 2385.
- [5] A.K. Cheetham, C.N.R. Rao, R.K. Feller, *Chem. Commun.* (2006) 4780.
- [6] O.K. Farha, J.T. Hupp, *Acc. Chem. Res.* 43 (2010) 1166.
- [7] S. Kitagawa, R. Matsuda, *Coord. Chem. Rev.* 251 (2007) 2490.
- [8] B.L. Chen, S.C. Xiang, G.D. Qian, *Acc. Chem. Res.* 43 (2010) 1115.
- [9] S.M. Cohen, Z.Q. Wang, *Chem. Soc. Rev.* 38 (2009) 1315.
- [10] Z.B. Ma, B. Moulton, *Coord. Chem. Rev.* 255 (2011) 1623.
- [11] C. Janiak, *Dalton Trans.* (2003) 2781.
- [12] S.M. Fang, E.C. Sanudo, M. Hu, Q. Zhang, S.T. Ma, L.R. Jia, C. Wang, J.Y. Tang, M. Du, C.S. Liu, *Cryst. Growth Des.* 11 (2011) 811.
- [13] R. Robson, *J. Chem. Soc. Dalton Trans.* (2000) 3735.
- [14] B. Moulton, M.J. Zaworotko, *Chem. Rev.* 101 (2001) 1629.
- [15] M. Eddaoudi, D.B. Moler, H. Li, B. Chen, T.M. Reineke, M. O'Keeffe, O.M. Yaghi, *Acc. Chem. Res.* 34 (2001) 319.
- [16] O.M. Yaghi, M. O'Keeffe, N.W. Ockwig, H.K. Chae, M. Eddaoudi, J. Kim, *Nature* 423 (2003) 705.
- [17] H. Liang, Q. Yu, X.P. Zhang, H.D. Bian, B. Zhao, S.P. Yan, D.Z. Liao, *Cryst. Growth Des.* 8 (2008) 1140.
- [18] L.S. Long, *CrystEngComm* 12 (2010) 1354.
- [19] B. Zheng, H. Dong, J.F. Bai, Y.Z. Li, S.H. Li, M. Scheer, *J. Am. Chem. Soc.* 130 (2008) 7778.
- [20] M. Du, C.P. Li, J.H. Guo, *CrystEngComm* 11 (2009) 1536.
- [21] C.P. Li, Q. Yu, J. Chen, M. Du, *Cryst. Growth Des.* 10 (2010) 2650.
- [22] C.P. Li, M. Du, *Chem. Commun.* 47 (2011) 5958.
- [23] D.F. Sun, S.Q. Ma, J.M. Simmons, J.R. Li, D.Q. Yuan, H.C. Zhou, *Chem. Commun.* 46 (2010) 1329.
- [24] H. Sakamoto, R. Matsuda, S. Bureekaew, D. Tanaka, S. Kitagawa, *Chem. Eur. J.* 15 (2009) 4985.
- [25] W. Guo, Y.Y. Yang, M. Du, *Inorg. Chem. Commun.* 13 (2010) 863.
- [26] G.R. Whittell, M.D. Hager, U.S. Schubert, I. Manners, *Nat. Mater.* 10 (2011) 176.
- [27] W.Y. Wong, P.D. Harvey, *Macromol. Rapid Commun.* 31 (2010) 671.
- [28] A.S. Aba-El-Aziz, P.O. Shipman, B.N. Boden, W.S. McNeil, *Prog. Polym. Sci.* 35 (2010) 714.
- [29] G.R. Whittell, I. Manners, *Adv. Mater.* 19 (2007) 3439.
- [30] W.Y. Wong, C.L. Ho, *Coord. Chem. Rev.* 250 (2006) 2627.
- [31] W.Y. Wong, *Dalton Trans.* (2007) 4495.
- [32] C.L. Ho, W.Y. Wong, *Coord. Chem. Rev.* 255 (2011) 2469.
- [33] S.M. Fang, M. Hu, L.R. Jia, C. Wang, Q. Zhang, S.T. Ma, M. Du, C.S. Liu, *CrystEngComm* 13 (2011) 6555.
- [34] J.R. Li, X.H. Bu, *Eur. J. Inorg. Chem.* (2008) 27.
- [35] W.Y. Wong, W.T. Wong, *J. Chem. Soc. Dalton Trans.* (1995) 2831.
- [36] M.A. Jalil, T. Yamada, S. Fujinami, T. Honjo, H. Nishikawa, *Polyhedron* 20 (2001) 627.
- [37] M. Kondo, T. Okubo, A. Asami, S. Noro, T. Yoshitomi, S. Kitagawa, T. Ishii, H. Matsuzaka, K. Seki, *Angew. Chem. Int. Ed.* 38 (1999) 140.
- [38] T.K. Maji, K. Uemura, H.C. Chang, R. Matsuda, S. Kitagawa, *Angew. Chem. Int. Ed.* 43 (2004) 3269.
- [39] B.J. Burnett, P.M. Barron, W. Choe, *CrystEngComm* 14 (2012) 3839.
- [40] M. Eddaoudi, H.L. Li, O.M. Yaghi, *J. Am. Chem. Soc.* 122 (2000) 1391.
- [41] H.K. Chae, D.Y. Siberio-Perez, J. Kim, Y. Go, M. Eddaoudi, A.J. Matzger, M. O'Keeffe, O.M. Yaghi, *Nature* 427 (2004) 523.
- [42] K. Koh, A.G. Wong-Foy, A.J. Matzger, *Angew. Chem. Int. Ed.* 47 (2008) 677.
- [43] L. Hou, J.P. Zhang, X.M. Chen, *Cryst. Growth Des.* 9 (2009) 2415.
- [44] M. O'Keeffe, M.A. Peskov, S.J. Ramsden, O.M. Yaghi, *Acc. Chem. Res.* 41 (2008) 1792.
- [45] D.N. Dybtsev, M.P. Yutkin, D.G. Samsonenko, V.P. Fedin, A.L. Nuzhdin, A.A. Bezrukova, K.P. Bryliakov, E.P. Talsi, R.V. Belosludov, H. Mizuseki, Y. Kawazoe, O.S. Subbotin, V.R. Belosludov, *Chem. Eur. J.* 16 (2010) 10348.
- [46] D.N. Dybtsev, A.L. Nuzhdin, H. Chun, K.P. Bryliakov, E.P. Talsi, V.P. Fedin, K. Kim, *Angew. Chem. Int. Ed.* 45 (2006) 916.
- [47] P.X. Yin, J.K. Cheng, Z.J. Li, L. Zhang, Y.Y. Qin, J. Zhang, Y.G. Yao, *Inorg. Chem.* 48 (2009) 10859.
- [48] Y.Y. Lin, J.P. Zhang, Y.B. Zhang, X.M. Chen, *Cryst. Growth Des.* 8 (2008) 3673.
- [49] Y. Qi, Y.X. Che, S.R. Batten, J.M. Zheng, *CrystEngComm* 10 (2008) 1027.
- [50] J. Tao, M.L. Tong, X.M. Chen, *J. Chem. Soc. Dalton Trans.* (2000) 3669.
- [51] F.P. Huang, J.L. Tian, G.J. Chen, D.D. Li, W. Gu, X. Liu, S.P. Yan, D.Z. Liao, P. Cheng, *CrystEngComm* 12 (2010) 1269.
- [52] J. Seo, C. Bonneau, R. Matsuda, M. Takata, S. Kitagawa, *J. Am. Chem. Soc.* 133 (2011) 9005.
- [53] T. Yamada, S. Iwakiri, T. Hara, K. Kanaizuka, M. Kurmoo, H. Kitagawa, *Cryst. Growth Des.* 11 (2011) 1798.
- [54] D. Liu, H.X. Li, Y. Chen, Y. Zhang, J.P. Lang, Chin. J. Chem. 26 (2008) 2173.
- [55] Z. Hulvey, J.D. Furman, S.A. Turner, M. Tang, A.K. Cheetham, *Cryst. Growth Des.* 10 (2010) 2041.
- [56] E. Yang, X.C. Song, Y.D. Lin, S.Z. Shen, *Acta Crystallogr. E63* (2007) m2067.
- [57] S.M. Chen, J. Zhang, C.Z. Lu, *CrystEngComm* 9 (2007) 389.
- [58] G.H. Wang, Z.G. Li, H.Q. Jia, N.H. Hu, J.W. Xu, *Cryst. Growth Des.* 8 (2008) 1932.
- [59] J. Zhang, Y.B. Chen, Z.J. Li, Y.Y. Qin, Y.G. Yao, *Inorg. Chem. Commun.* 9 (2006) 449.
- [60] Y.P. Diao, K. Li, S.S. Huang, X.H. Shu, X. Liu, X.M. Deng, *Acta Crystallogr. C65* (2009) m82.
- [61] Z.F. Tian, J.G. Lin, Y. Su, L.I. Wen, Y.M. Liu, H.Z. Zhu, Q.J. Meng, *Cryst. Growth Des.* 7 (2007) 1863.
- [62] A. Schaate, S. Klingelhofer, P. Behrens, M. Wiebecke, *Cryst. Growth Des.* 8 (2008) 3200.
- [63] G.H. Wei, J. Yang, J.F. Ma, Y.Y. Liu, S.L. Li, L.P. Zhang, *Dalton Trans.* (2008) 3080.
- [64] Y. Qi, Y.X. Che, J.M. Zheng, *CrystEngComm* 10 (2008) 1137.
- [65] B.L. Li, B.Z. Li, X. Zhu, X.H. Lu, Y. Zhang, *J. Coord. Chem.* 57 (2004) 1361.
- [66] J. Wang, X. Zhu, Y.F. Cui, B.L. Li, H.Y. Li, *CrystEngComm* 13 (2011) 3342.
- [67] X.L. Wang, C. Qin, E.B. Wang, Z.M. Su, *Chem. Eur. J.* 12 (2006) 2680.
- [68] J.Y. Hu, J.P. Li, J.A. Zhao, H.W. Hou, Y.T. Fan, *Inorg. Chim. Acta* 362 (2009) 5023.
- [69] L. Zhang, Y. Ling, D.J. Li, J. Li, M. Du, *Inorg. Chim. Acta* 363 (2010) 1031.
- [70] L. Xu, G.C. Guo, B. Liu, M.S. Wang, J.S. Huang, *Inorg. Chem. Commun.* 7 (2004) 1145.
- [71] J. Tao, M.L. Tong, J.X. Shi, X.M. Chen, S.W. Ng, *Chem. Commun.* (2000) 2043.
- [72] Y.M. Dai, E. Ma, E. Tang, J. Zhang, Z.J. Li, X.D. Huang, Y.G. Yao, *Cryst. Growth Des.* 5 (2005) 1313.
- [73] S. Horike, D. Tanaka, K. Nakagawa, S. Kitagawa, *Chem. Commun.* (2007) 3395.
- [74] Y. Hijikata, S. Horike, M. Sugimoto, H. Sato, R. Matsuda, S. Kitagawa, *Chem. Eur. J.* 17 (2011) 5138.
- [75] S.A. Bourne, J.J. Lu, B. Moulton, M.J. Zaworotko, *Chem. Commun.* (2001) 861.
- [76] H.Y. Liu, H. Wu, J.F. Ma, Y.Y. Liu, B. Liu, J. Yang, *Cryst. Growth Des.* 10 (2010) 4795.
- [77] Y.A. Simonov, S.G. Baca, I.G. Filippova, M. Gdaniec, O.A. Gerko, N.V. Gerbeleu, *Russ. J. Coord. Chem.* 30 (2004) 727.
- [78] Y.Q. Zheng, J. Zhang, J.Y. Liu, *CrystEngComm* 12 (2010) 2740.
- [79] Y.Q. Gong, R.H. Wang, D.Q. Yuan, W.P. Su, Y.G. Huang, C.Y. Yue, F.L. Jiang, M.C. Hong, *Polyhedron* 26 (2007) 5309.
- [80] S.M. Fang, Q. Zhang, M. Hu, X.G. Yang, L.M. Zhou, M. Du, C.S. Liu, *Cryst. Growth Des.* 10 (2010) 4773.
- [81] S.M. Fang, M. Hu, Q. Zhang, M. Du, C.S. Liu, *Dalton Trans.* 40 (2011) 4527.
- [82] P. Mahata, G. Madras, S. Natarajan, *J. Phys. Chem. B* 110 (2006) 13759.
- [83] S. Pramanik, C. Zheng, X. Zhang, T.J. Emge, J. Li, *J. Am. Chem. Soc.* 133 (2011) 4153.
- [84] J. Tao, J.X. Shi, M.L. Tong, X.X. Zhang, X.M. Chen, *Inorg. Chem.* 40 (2001) 6328.
- [85] J. Li, Y. Peng, H.W. Liang, Y. Yu, B.J. Xin, G.H. Li, Z. Shi, S.H. Feng, *Eur. J. Inorg. Chem.* (2011) 2712.
- [86] W.Y. Wong, S.H. Cheung, S.M. Lee, S.Y. Leung, *J. Organomet. Chem.* 596 (2000) 36.
- [87] M. Kondo, Y. Irie, M. Miyazawa, H. Kawaguchi, S. Yasue, K. Maeda, F. Uchida, *J. Organomet. Chem.* 692 (2007) 136.
- [88] L.F. Ma, Q.L. Meng, C.P. Li, B. Li, L.Y. Wang, M. Du, F.P. Liang, *Cryst. Growth Des.* 10 (2010) 3036.
- [89] L.F. Ma, C.P. Li, L.Y. Wang, M. Du, *Cryst. Growth Des.* 10 (2010) 2641.
- [90] L.F. Ma, B. Liu, L.Y. Wang, J.L. Hu, M. Du, *CrystEngComm* 12 (2010) 1439.
- [91] L.F. Ma, Q.L. Meng, L.Y. Wang, B. Liu, F.P. Liang, *Dalton Trans.* 39 (2010) 8210.
- [92] Z.J. Lin, T.F. Liu, B. Xu, L.W. Han, Y.B. Huang, R. Cao, *CrystEngComm* 13 (2011) 3321.
- [93] X.L. Wang, C. Qin, E.B. Wang, L. Xu, *J. Mol. Struct.* 737 (2005) 49.
- [94] J. Tao, X.M. Chen, R.B. Huang, L.S. Zheng, *J. Solid State Chem.* 170 (2003) 130.
- [95] J.J. Zhang, L. Wojtas, R.W. Larsen, M. Eddaoudi, M.J. Zaworotko, *J. Am. Chem. Soc.* 131 (2009) 17040.
- [96] M. Du, X.J. Jiang, X.J. Zhao, *Inorg. Chem.* 46 (2007) 3984.
- [97] M. Du, X.J. Jiang, X.J. Zhao, *Chem. Commun.* (2005) 5521.
- [98] Q.F. He, D.S. Li, J. Zhao, X.J. Ke, C. Li, Y.Q. Mou, *Inorg. Chem. Commun.* 14 (2011) 578.
- [99] M. Du, X.H. Bu, *Bull. Chem. Soc. Jpn.* 82 (2009) 539.
- [100] M. Du, Q. Wang, C.P. Li, X.J. Zhao, J. Ribas, *Cryst. Growth Des.* 10 (2010) 3285.
- [101] F.P. Huang, J.L. Tian, W. Gu, X. Liu, S.P. Yan, D.Z. Liao, P. Cheng, *Cryst. Growth Des.* 10 (2010) 1145.
- [102] M. Du, Z.H. Zhang, Y.P. You, X.J. Zhao, *CrystEngComm* 10 (2008) 306.
- [103] J.J. Liu, X. He, M. Shao, M.X. Li, *J. Mol. Struct.* 891 (2008) 50.
- [104] C.P. Li, J. Chen, M. Du, *Polyhedron* 29 (2010) 463.
- [105] S.M. Fang, Q. Zhang, M. Hu, B. Xiao, L.M. Zhou, G.H. Sun, L.J. Gao, M. Du, C.S. Liu, *CrystEngComm* 12 (2010) 2203.
- [106] Z.H. Zhang, S.C. Chen, J.L. Mi, M.Y. He, Q. Chen, M. Du, *Chem. Commun.* 46 (2010) 8427.
- [107] L.F. Ma, Y.Y. Wang, J.Q. Liu, G.P. Yang, M. Du, L.Y. Wang, *CrystEngComm* 11 (2009) 1800.
- [108] J. Chen, C.P. Li, M. Du, *CrystEngComm* 13 (2011) 1885.
- [109] J.H. Guo, J. Chen, C.P. Li, M. Du, *J. Mol. Struct.* 975 (2010) 147.

- [110] Q. Yu, C.P. Li, Z.H. Zhang, M. Du, *Polyhedron* 28 (2009) 2347.
- [111] M. Du, C.P. Li, X.J. Zhao, *CrystEngComm* 8 (2006) 552.
- [112] C.P. Li, J. Chen, Q. Yu, M. Du, *Cryst. Growth Des.* 10 (2010) 1623.
- [113] M. Du, X.J. Zhao, J.H. Guo, S.R. Batten, *Chem. Commun.* (2005) 4836.
- [114] M. Du, X.G. Wang, Z.H. Zhang, L.F. Tang, X.J. Zhao, *CrystEngComm* 8 (2006) 788.
- [115] Y.Y. Yang, W. Guo, M. Du, *Inorg. Chem. Commun.* 13 (2010) 1195.
- [116] S.C. Chen, Z.H. Zhang, K.L. Huang, Q. Chen, M.Y. He, A.J. Cui, C. Li, Q. Liu, M. Du, *Cryst. Growth Des.* 8 (2008) 3437.
- [117] X.D. Chen, M. Du, T.C.W. Mak, *Chem. Commun.* (2005) 4417.
- [118] M. Du, C.P. Li, J.M. Wu, J.H. Guo, G.C. Wang, *Chem. Commun.* 47 (2011) 8088.
- [119] X.D. Chen, X.H. Zhao, M. Chen, M. Du, *Chem. Eur. J.* 15 (2009) 12974.
- [120] X. Li, R. Cao, W.H. Bi, D.Q. Yuan, D.F. Sun, *Eur. J. Inorg. Chem.* (2005) 3156.
- [121] B.L. Chen, C.D. Liang, J. Yang, D.S. Contreras, Y.L. Clancy, E.B. Lobkovsky, O.M. Yaghi, S. Dai, *Angew. Chem. Int. Ed.* 45 (2006) 1390.
- [122] H. Wang, Y.Y. Wang, G.P. Yang, C.J. Wang, G.L. Wen, Q.Z. Shi, S.R. Batten, *CrystEngComm* 10 (2008) 1583.
- [123] X.D. Chen, H.F. Wu, X.H. Zhao, X.J. Zhao, M. Du, *Cryst. Growth Des.* 7 (2007) 124.
- [124] X.J. Jiang, S.Z. Zhang, J.H. Guo, X.G. Wang, J.S. Li, M. Du, *CrystEngComm* 11 (2009) 855.
- [125] M. Du, C.P. Li, X.J. Zhao, *Cryst. Growth Des.* 6 (2006) 335.
- [126] C.P. Li, M. Du, *Inorg. Chem. Commun.* 14 (2011) 502.
- [127] C.P. Li, J. Chen, M. Du, *CrystEngComm* 12 (2010) 4392.
- [128] M. Du, X.J. Jiang, X.J. Zhao, *Inorg. Chem.* 45 (2006) 3998.
- [129] X.D. Chen, H.F. Wu, M. Du, *Chem. Commun.* (2008) 1296.
- [130] H.T. Xu, Y.D. Li, *J. Mol. Struct.* 693 (2004) 11.
- [131] J. Tao, X. Yin, Y.B. Jiang, L.F. Yang, R.B. Huang, L.S. Zheng, *Eur. J. Inorg. Chem.* (2003) 2678.
- [132] T. Fukushima, S. Horike, Y. Inubushi, K. Nakagawa, Y. Kubota, M. Takata, S. Kitagawa, *Angew. Chem. Int. Ed.* 49 (2010) 4820.
- [133] L.F. Ma, L.Y. Wang, M. Du, S.R. Batten, *Inorg. Chem.* 49 (2010) 365.
- [134] J. Yang, B. Li, J.F. Ma, Y.Y. Liu, J.P. Zhang, *Chem. Commun.* 46 (2010) 8383.
- [135] X.J. Ke, D.S. Li, M. Du, *Inorg. Chem. Commun.* 14 (2011) 788.
- [136] D.S. Li, Y.P. Wu, P. Zhang, M. Du, J. Zhao, C.P. Li, Y.Y. Wang, *Cryst. Growth Des.* 10 (2010) 2037.
- [137] X.L. Wang, H.L. Hu, G.C. Liu, H.Y. Lin, A.X. Tian, *Chem. Commun.* 46 (2010) 6485.
- [138] L.F. Ma, L.Y. Wang, Y.Y. Wang, S.R. Batten, J.G. Wang, *Inorg. Chem.* 48 (2009) 915.
- [139] L.F. Ma, B. Liu, L.Y. Wang, C.P. Li, M. Du, *Dalton Trans.* 39 (2010) 2301.
- [140] D.S. Li, F. Fu, J. Zhao, Y.P. Wu, M. Du, K. Zou, W.W. Dong, Y.Y. Wang, *Dalton Trans.* 39 (2010) 11522.
- [141] R.E. Morris, X.H. Bu, *Nat. Chem.* 2 (2010) 353.
- [142] R.E. Morris, *Chem. Commun.* (2009) 2990.
- [143] E.R. Cooper, C.D. Andrews, P.S. Wheatley, P.B. Webb, P. Wormald, R.E. Morris, *Nature* 430 (2004) 1012.
- [144] J. Zhang, S.M. Chen, T. Wu, P.Y. Feng, X.H. Bu, *J. Am. Chem. Soc.* 130 (2008) 12882.
- [145] C.P. Li, J.M. Wu, M. Du, *Inorg. Chem.* 50 (2011) 9284.
- [146] Z. Su, J. Fan, T. Okamura, W.Y. Sun, N. Ueyama, *Cryst. Growth Des.* 10 (2010) 3515.
- [147] R. Vaidhyanathan, D. Bradshaw, J.N. Rebill, J.P. Barrio, J.A. Gould, N.G. Berry, M.J. Rosseinsky, *Angew. Chem. Int. Ed.* 45 (2006) 6495.
- [148] D.N. Dybtsev, M.P. Yutkin, E.V. Peresypkina, A.V. Virovets, C. Serre, G. Ferey, V.P. Fedin, *Inorg. Chem.* 46 (2007) 6843.
- [149] J. Zhang, R. Liu, P.Y. Feng, X.H. Bu, *Angew. Chem. Int. Ed.* 46 (2007) 8388.
- [150] J. Zhang, X.H. Bu, *Angew. Chem. Int. Ed.* 46 (2007) 6115.
- [151] S.C. Xiang, Z.J. Zhang, C.G. Zhao, K.L. Hong, X.B. Zhao, D.R. Ding, M.H. Xie, C.D. Wu, M.C. Das, R. Gill, K.M. Thomas, B.L. Chen, *Nat. Commun.* 2 (2011) 204.
- [152] J.R. Li, R.J. Kuppler, H.C. Zhou, *Chem. Soc. Rev.* 38 (2009) 1477.
- [153] J.R. Li, J. Sculley, H.C. Zhou, *Chem. Rev.* 112 (2012) 869.
- [154] D. MasPOCH, D. Ruiz-Molina, J. Veciana, *Chem. Soc. Rev.* 36 (2007) 770.
- [155] M. Yoon, R. Srirambalaji, K. Kim, *Chem. Rev.* 112 (2012) 1196.
- [156] K. Sumida, D.L. Rogow, J.A. Mason, T.M. McDonald, E.D. Bloch, Z.R. Herm, T.H. Bae, J.R. Long, *Chem. Rev.* 112 (2012) 724.
- [157] Y. Liu, W. Xuan, Y. Cui, *Adv. Mater.* 22 (2010) 4112.
- [158] B.L. Chen, S.Q. Ma, F. Zapata, F.R. Fronczeck, E.B. Lobkovsky, H.C. Zhou, *Inorg. Chem.* 46 (2007) 1233.
- [159] B.Q. Ma, K.L. Mulfort, J.T. Hupp, *Inorg. Chem.* 44 (2005) 4912.
- [160] S.I. Vagin, A.K. Ott, S.D. Hoffmann, D. Lanzinger, B. Rieger, *Chem. Eur. J.* 15 (2009) 5845.
- [161] Z. Chang, D.S. Zhang, Q. Chen, R.F. Li, T.L. Hu, X.H. Bu, *Inorg. Chem.* 50 (2011) 7555.
- [162] H. Chun, D.N. Dybtsev, H. Kim, K. Kim, *Chem. Eur. J.* 11 (2005) 3521.
- [163] R. Kitaura, K. Seki, G. Akiyama, S. Kitagawa, *Angew. Chem. Int. Ed.* 42 (2003) 428.
- [164] R. Kitaura, K. Fujimoto, S. Noro, M. Kondo, S. Kitagawa, *Angew. Chem. Int. Ed.* 41 (2002) 133.
- [165] J. Pasán, J. Sanchiz, F. Lloret, M. Julve, C. Ruiz-Pérez, *CrystEngComm* 9 (2007) 478.
- [166] F.S. Delgado, J. Sanchiz, C. Ruiz-Pérez, F. Lloret, M. Julve, *Inorg. Chem.* 42 (2003) 5938.
- [167] H. Tian, Q.X. Jia, E.Q. Gao, Y.Q. Wang, *Chem. Commun.* 46 (2010) 5349.
- [168] Y.Q. Zheng, J.L. Lin, Z.P. Kong, *Inorg. Chem.* 43 (2004) 2590.
- [169] V.I. Isaeva, L.M. Kustov, *Petrol. Chem.* 50 (2010) 167.
- [170] A. Corma, H. Garcia, F.X.L. Xamena, *Chem. Rev.* 110 (2010) 4606.
- [171] Z.T. Yu, Z.L. Liao, Y.S. Jiang, G.H. Li, G.D. Li, J.S. Chen, *Chem. Commun.* (2004) 1814.
- [172] T. Uemura, R. Kitaura, Y. Ohta, M. Nagaoka, S. Kitagawa, *Angew. Chem. Int. Ed.* 45 (2006) 4112.
- [173] R. Matsuda, R. Kitaura, S. Kitagawa, Y. Kubota, R.V. Belosludov, T.C. Kobayashi, H. Sakamoto, T. Chiba, M. Takata, Y. Kawazoe, Y. Mita, *Nature* 436 (2005) 238.